STEM CELLS

STEM CELL GENETICS AND GENOMICS

Microarray Analyses Support a Role for Nurr1 in Resistance to Oxidative Stress and Neuronal Differentiation in Neural Stem Cells

KYLE M. SOUSA,[a] HELENA MIRA,[a,d] ANITA C. HALL,[a,b] LOTTIE JANSSON-SJÖSTRAND,[a] MORIAKI KUSAKABE,[c] ERNEST ARENAS[a]

[a]Laboratory of Molecular Neurobiology, Department of Medical Biochemistry and Biophysics, Karolinska Institute, Stockholm, Sweden; [b]Division of Cell and Molecular Biology, Imperial College London, London, United Kingdom; [c]Experimental Animal Research Center, Institute for Animal Reproduction, Ibaraki, Japan; [d]Stem Cell Regulation Laboratory, Prince Felipe Research Center, Valencia, Spain

Key Words. Nuclear receptor • Dopamine • Nurr1 • Parkinson disease • Stem cells

ABSTRACT

Nurr1 is an orphan nuclear receptor required for the development of midbrain dopaminergic neurons. To better understand the molecular consequences of Nurr1 expression, we compared the transcriptomes of two independent control and Nurr1-expressing NSC lines using Affymetrix cDNA microarrays. These data reveal the regulation of genes involved in promoting cell survival (trophic/growth factors and stress response genes) and in preventing cell death (decreased caspase-3 and caspase-11 expression). We found that conditioned medium from Nurr1-expressing NSC lines enhanced the survival of midbrain dopaminergic neurons in primary cultures and that Nurr1-expressing NSC lines themselves were more resistant to oxidative stress. These findings are accompanied by a dynamic pattern of gene regulation that is consistent with a role for Nurr1 in promoting both the acquisition of brain-region-specific identity (Engrailed-1) and neuronal differentiation (tubulin β III). Interestingly, our gene expression profiles suggested that tenascin-C was regulated by Nurr1 in developing dopaminergic neurons. This was further confirmed in vitro and in Nurr1 knockout mice where low levels of tenascin-C mRNA were observed. Analysis of tenascin-C-null mice revealed an increase in the number of Nurr1$^+$ cells that become tyrosine hydroxylase-positive (TH$^+$) dopaminergic neurons at embryonic day 11.5, suggesting that tenascin-C normally delays the acquisition of TH by Nurr1$^+$ precursors. Thus, our results confirm the presence of both secreted and cell-intrinsic survival signals modulated by Nurr1 and suggest that Nurr1 is a key regulator of both survival and dopaminergic differentiation. STEM CELLS *2007;25:511–519*

INTRODUCTION

Parkinson disease (PD), the second most common human neurodegenerative disorder, primarily results from the selective and progressive degeneration of ventral midbrain dopamine-synthesizing neurons. Cell-replacement strategies based on the transplantation of stem cells manipulated to efficiently generate functional dopaminergic neurons have recently raised hope for the improved treatment of PD patients. In addition, genetic engineering of mouse neural stem cells and ESCs using nuclear receptor related-1 (Nurr1/NR4A2) has proven successful for generating cell populations enriched in dopaminergic (DA) neurons [1–3]. Despite the therapeutic potential of these engineered cells for patients with PD, the function of Nurr1 in genetically engineered stem cells remains unclear.

Nurr1 is a transcription factor of the nuclear receptor superfamily that is highly expressed in the developing and adult ventral midbrain [4]. In the midbrain, Nurr1 is detected prior to the expression of tyrosine hydroxylase (TH) in dopaminergic neurons in vivo [5–7]. Moreover, in Nurr1-null mice, midbrain TH$^+$ neurons are not born, and in their usual position, cells die by apoptosis at embryonic day 18.5 (E18.5) [5, 8]. These studies suggest that Nurr1 is required for both the specification of neurotransmitter phenotype and for neuronal differentiation/survival. In agreement with these data, we have previously demonstrated that Nurr1 overexpression induces neuronal differentiation in the c17.2 NSC line [3]. However, Nurr1 NSCs adopt a TH$^+$ dopaminergic phenotype only upon coculture with embryonic/newborn midbrain astrocytes, suggesting that additional non-cell-autonomous signals, including Wnt-5a, are required for dopaminergic differentiation [3, 9, 10]. The c17.2 NSC line consists of multipotent neural progenitors isolated from the external germinal layer of the cerebellum [11]. This cell line was initially immortalized using retroviral v-myc transfer and differentiates into both glial and neuronal cell types upon transplantation into various central nervous system regions.

Nurr1 is expressed in adult neurons and is regulated by different types of brain insults, including ischemia [12] and seizures [13, 14]. These results, together with an increased loss of dopaminergic neurons in Nurr1$^{+/-}$ mice [15], have suggested a role for Nurr1 in neuronal survival after the birth of dopaminergic neurons. To gain more insights into the molecular events elicited by exogenous Nurr1 expression in stem cells, we have analyzed the transcription profile of c17.2 neural stem cells stably transfected with Nurr1. Here, we show that Nurr1 exerts multiple functions, including facilitating the differentiation of multipotent stem cells, maintaining postmitotic neuronal precur-

Correspondence: Ernest Arenas, M.D., Ph.D., Karolinska Institute, Division of Molecular Neurobiology, MBB, Scheeles väg 1, A1 Plan 2, Stockholm 17177, Sweden. Telephone: 46-8-728-7663; Fax: 46-8-341960; e-mail: ernest.arenas@mbb.ki.se Received April 20, 2006; accepted for publication September 29, 2006; first published online in STEM CELLS *EXPRESS* October 12, 2006. 1066-5099/2007/$30.00/0 doi: 10.1634/stemcells.2006-0238

sor populations, promoting survival, and conferring resistance to oxidative stress.

MATERIALS AND METHODS

Cell Culture and Treatment

c17.2 neural stem cells were maintained and passaged as previously described [11]. To generate accumulated cell growth curves, the total number of viable cells was assessed at each passage by trypan blue exclusion, and 500,000 viable cells were plated. At the time of the next passage (after 2 days in vitro), the number of cells generated was determined, and the ratio of cell production was multiplied by the total number of cells in the previous point of the curve. Growth data are represented by the equation $y = a \cdot 2^{sx}$, where y is the total number of cells, x is the time in days in vitro (DIV), s is the rate of doubling, and a is a constant [16]. For differentiation, c17.2 cells were plated on poly(D-lysine)-coated wells in a defined, serum-free medium (N2, consisting of a 1:1 mixture of Ham's F-12 and minimal essential medium supplemented with 15 mM HEPES buffer, 5 μg/ml insulin, 100 μg/ml apo-transferrin, 100 μM putrescine, 20 nM progesterone, 30 nM selenium, 6 mg/ml glucose, and 1 mg/ml bovine serum albumin (BSA), and grown for 3 DIV. Cells were fixed with 4% paraformaldehyde (PFA) for 20 minutes prior to immunocytochemical analysis. For primary cultures, ventral mesencephala from E12.5 mouse embryos were dissected, treated with dispase/DNase, mechanically dissociated, and plated at a density of 125,000 cells per cm^2 in N2 medium supplemented with 20 ng/ml basic fibroblast growth factor for 2 hours. Medium was then changed to 0.2-μm-filtered N2 that had been conditioned by c17.2 cells for 24 hours.

RNA Preparation, Real-Time Reverse Transcription-Polymerase Chain Reaction, and Quantification of Gene Expression

RNA from c17.2 cells was extracted using RNeasy Mini Kit (Qiagen, Hilden, Germany, http://www1.qiagen.com). Five μg of total RNA from two control (puroB [pB] and puroD [pD]) and two Nurr1-overexpressing cell lines (clone 42 [c42] and clone 48 [c48]) was treated with RQ1 RNase-free DNase (Promega, Madison, WI, http://www.promega.com), and RNA integrity was assessed by electrophoresis. RNA was also prepared from dissected ventral mesencephala of E11 wild-type and Nurr1-null embryos. Briefly, 1 μg of RNA was reverse-transcribed using SuperScript II Reverse Transcriptase (Invitrogen) and random primers (Invitrogen, Carlsbad, CA, http://www.invitrogen.com) (reverse transcription-positive [RT^+] reaction), and parallel reactions without reverse transcriptase enzyme were done as a control (RT^- reaction). Quantitative polymerase chain reaction (PCR) was performed as previously described [10].

High-Density Oligonucleotide Array Hybridization

RNA probes were labeled according to the supplier's instructions (Affymetrix, Santa Clara, CA, http://www.affymetrix.com). First-strand synthesis was carried out by a T7-(dT)24 primer and SuperScript II reverse transcriptase (Gibco-BRL, Gaithersburg, MD, http://www.gibcobrl.com) using 10 μg of total RNA sample. Second-strand synthesis was performed according to the SuperScript Choice System (Gibco-BRL) by *Escherichia coli* DNA-polymerase I, *E. coli* ligase, and RNase H. Fragment end polishing was performed using T4-polymerase. An in vitro transcription reaction was used to incorporate biotin-11-CTP and biotin-16-UTP into the cRNA probe (BioArray HighYield RNA Transcript Labeling Kit; Enzo Life Sciences, Farmingdale, NY, http://www.enzolifesciences.com). The fragmented cRNA was hybridized overnight (45°C) to the DNA chips. Washes were done in the GeneChip Fluidics Station (Affymetrix) according to the manufacturer's protocol. Staining was performed with R-phycoerythrin streptavidin (Molecular Probes Inc., Eugene, OR, http://probes.invitrogen.com), followed by an antibody amplification procedure using biotinylated anti-streptavidin antibody (Vector Laboratories, Burlingame, CA, http://www.vectorlabs.com) and goat IgG (Sigma-Aldrich, St. Louis, http://www.sigmaaldrich.com). The scanning was carried out at 3 μm resolution, 488 nm excitation, and 570 nm emission wavelengths using the GeneArray Scanner (Hewlett Packard, Palo Alto, CA, http://www.hewlettpackard.com). Two control (pB and pD) and two Nurr1-overexpressing (c42 and c48) cell lines were processed independently. Data were scaled based on total intensity, and data analysis was performed with Affymetrix software (MAS 5.0). The p values were calculated by applying the Wilcoxon's signed rank test and then used to generate the complex calls. Complete microarray data were registered at the National Center for Biotechnology Information (NCBI) Gene Expression Omnibus (GEO) and hybridization array data repository as GSE3571 (http://www.ncbi.nlm.nih.gov/geo).

Immunocytochemical Analysis

Cultures were blocked for 1 hour at room temperature in PBST (1× phosphate-buffered saline [PBS], 1% BSA, and 0.3% Triton X-100) and overnight at 4°C with the corresponding primary antibody diluted in blocking buffer. The following antibodies were used: mouse anti-β-tubulin type-III (TuJ1), 1:2,000 (Sigma-Aldrich); mouse anti-TH, 1:10,000 (Diasorin, Stillwater, MN, http://www.diasorin.com); mouse anti-Engrailed-1 (1:50), rabbit anti-glial fibrillary acidic protein, 1:500 (DAKO, Glostrup, Denmark, http://www.dako.com); rabbit anti-tenascin-C (TN-C), 1:250 (Chemicon, Temecula, CA, http://www.chemicon.com); mouse anti-cleaved caspase-3 (Asp175), 1:100 (Cell Signaling Technology, Beverly, MA, http://www.cellsignal.com); and mouse Nestin (Rat-401), 1:500 (Developmental Studies Hybridoma Bank, University of Iowa). After washing, cultures were incubated with biotinylated secondary antibodies diluted 1:500 for 2 hours, and immunostaining was visualized using Vector Laboratories ABC immunoperoxidase kit and Supergrey substrate. For immunofluorescence, 1:100 dilutions of Cy2- or rhodamine-coupled secondary antibodies (Jackson Immunoresearch Laboratories, West Grove, PA, http://www.jacksonimmuno.com) were used. Cultures were then rinsed twice in PBS and analyzed.

Cell Death and Oxidative Stress Assays

For oxidative stress experiments, c17.2 cells were grown to 60% confluence, plated at a density of 5,000 cells per cm^2, and allowed to grow overnight. The following day, fresh medium was added, and cells were treated with freshly diluted 25 μM H_2O_2 for 0 or 6 hours. Following peroxide treatment, cells were fixed with 4% PFA for 20 minutes, rinsed, and blocked with PBS/5% goat serum for 30 minutes at room temperature. Immunocytochemistry for cleaved caspase-3 was performed as described above. Next a 1:500 dilution of Hoechst 33328 (0.5 mg/ml) was added for 5 minutes at room temperature. Cells were washed twice in PBS, visualized under a Zeiss HBO100 microscope (Carl Zeiss, Jena, Germany, http://www.zeiss.com), and counted. For cell viability assays, cell lines were grown, plated, and treated as described above. Cells were stained with 100 μg/ml Hoechst 33342 and 2 μg/ml propidium iodide in ice-cold PBS. After 10 minutes, the unfixed, stained cells were immediately counted.

Tenascin-C Knockout Mice and Immunohistochemistry

TN-C-null mice were previously described [17, 18]. Embryos were fixed in ice-cold 4% PFA for 6 hours, cryoprotected in 20% sucrose, and frozen in OCT compound at −70°C. Next, serial coronal 14 μM sections of the entire ventral midbrain were cut on a cryostat. Immunohistochemistry was performed on 4% paraformaldehyde-postfixed slides. Incubations were carried out at 4°C overnight with the following antibodies diluted in PBS, pH 7.3, 1% BSA, and 0.3% Triton X-100 solution: rabbit anti-Nurr1 (1:500 dilution; Santa Cruz Biotechnology Inc., Santa Cruz, CA, http://www.scbt.com), rabbit anti-TH (1:1,000; Pel-Freeze Biologicals, Rogers, AR, http://www.pelfreez-bio.com), rat anti-bromodeoxyuridine (BrdU) (1:200; Abcam, Cambridge, U.K., http://www.abcam.com), mouse anti-phosphorylated histone H3 (Ser10) (1:100; Upstate, Charlottesville, VA, http://www.upstate.com), mouse anti-RC2 (1:200; DSHB), guinea

pig anti-glutamate transporter, GLAST (1:2,000; Chemicon). After washes, the sections were blocked for 30 minutes in dilution buffer and then incubated for 2–4 hours with a secondary antibody (Cy2/3 [cyanine]-coupled donkey anti-mouse IgG, Cy2-coupled donkey anti-rabbit IgG [1:200 dilution; Jackson Immunoresearch Laboratories]). Immunostaining was visualized by using a Zeiss HBO100 microscope. For BrdU analysis, pregnant mice were injected with 0.5 ml of a 1 mg/ml BrdU/saline solution 6 hours before sacrifice. Pretreatment with 2 N HCl for 15 minutes prior to preincubation with primary antibody was needed for detection of BrdU. Stainings were visualized using a Zeiss HBO100 microscope, and images were collected with a Hamamatsu C4742-95 camera (Bridgewater, NJ, http://www.hamamatsu.com).

RESULTS

Microarray Analysis of Nurr1 Neural Stem Cells

Although overexpression of Nurr1 facilitates the differentiation of neural stem cells [3] and ESCs [1, 2] into midbrain DA neurons, the effects of Nurr1 on downstream gene expression in a proliferating cell remain unclear. To investigate this, we determined the transcription profile of proliferating c17.2 neural stem cell lines stably transfected with Nurr1 [3]. Two Nurr1-overexpressing clones, clone 42 and clone 48, and two control clones transfected with a control vector, pB and pD, were chosen for this study. Clone 42 and clone 48 were selected among all the Nurr1-transfected cell lines generated because of their high potential to become TH^+ dopaminergic neurons upon coculture with immature ventral mesencephalic glia [3]. Accumulated in vitro cell growth curves were generated (supplemental online Fig. 1A), and population doubling rates (PoDs) (the reciprocal of the doubling time in DIV) for the clones were estimated from these curves (PoD = 0.57 ± 0.05 for clone 42; PoD = 0.84 ± 0.02 for clone 48; PoD = 0.53 ± 0.09 for clone pB; PoD = 0.75 ± 0.01 for clone pD). To minimize the effects of proliferation on the study, the Nurr1 and corresponding control clones were matched (c42 with pB and c48 with pB) according to their doubling rates and further processed for gene expression comparison (supplemental online Fig. 1A).

The overall gene expression pattern of c42 versus clone pB and of c48 versus clone pD was compared using the Affymetrix murine U74v2 type A microarray. Total RNA from the c17.2 clones was isolated, reverse-transcribed, and hybridized to the chip. Of the >12,000 genes queried, a total of 1,949 genes were upregulated (1,081 in the c42/pB subtraction and 868 in the c48/pD subtraction), whereas 2,502 genes were downregulated (1,472 in c42/pB and 1,030 in c48/pD). However, only those genes regulated in a coordinate manner between the two independent comparisons were considered for further validation and quantitative analysis. These genes included 190 activated genes and 203 repressed genes (supplemental online Fig. 1B).

Classification and Confirmation of Genes Regulated by Nurr1 in Neural Stem Cells

The distribution of identified genes with known or putative functions is shown in supplemental online Figure 1C, and a complete list is available online (NCBI/GEO GSE3571). The highest number of genes up- and downregulated represented expressed sequence tags (23%) whose functions are unknown. The majority of characterized genes regulated encoded transcription factors (11%) and proteins involved in intracellular signaling (15%). The expression of several secreted ligand (3%)-inducing growth factors and extracellular matrix/cell adhesion molecules (13%) was also regulated. In addition, Nurr1 overexpression downregulated a number of cell cycle genes (4%), including cyclin B2, D1, and p21, whose regulation has been implicated in the differentiation of ventral progenitors [19]. Nurr1 overexpression also resulted in the upregulation of trophic/survival signals that coincided with the downregulation of a number of proapoptotic genes (10%) (downregulation of caspase-3 and -11). For a more detailed analysis, we focused our studies on those genes either up- or downregulated at least twofold or an average of 2.5-fold in both of the independent comparisons and classified them by broad biological function (Tables 1, 2, respectively). Many genes were represented several times in the chip and showed concordant expression, thereby validating the hybridization. To confirm the results of the microarray, 11 genes were randomly selected for quantitative PCR analysis either in the respective clones or in c17.2 neural stem cells transiently transfected with Nurr1 (data not shown). We found that in virtually all cases analyzed (10 of 11), the selected genes were corroborated (Table 3). To extend the validation of our microarray analysis further, we analyzed the expression of eight selected genes in three additional Nurr1-expressing clones: clones 12 (c12), 19 (c19), and 26 (c26). We observed that in all cases except one, the genes regulated in c42 and c48 were also regulated in c12, c19, and c26 (supplemental online Fig. 2). These data, obtained in five independent Nurr1-expressing clones, confirm that several of the genes identified in the array are regulated by Nurr1.

Nurr1 Induces the Expression of Neuronal Markers in NSCs

Several lines of evidence, including our microarray, have suggested distinct functions for Nurr1 in neuronal differentiation [20, 21]. To investigate the effects of Nurr1 in this process, we stained both control and Nurr1 NSC clones with several markers that define stages of progressive neuronal differentiation. Both control and Nurr1 NSCs stained positive for the neural stem cell marker Nestin (Fig. 1A). However, Nurr1-overexpressing clones exhibited higher levels of immunoreactivity for the neuronal cytoskeletal protein Tuj1 and Engrailed-1 (Fig. 1A), both upregulated 4- and 2.4-fold, respectively, in the microarray. Nurr1-overexpressing NSCs were also immunoreactive for TN-C, an extracellular matrix protein critical for the development and maintenance of several neuronal types [17, 18] (Fig. 1B). Consistent with these observations was the finding that virtually all Nurr1-overexpressing cells, but not control cells, acquired a bipolar neuronal morphology and were double-labeled with antibodies against Tuj1 and TN-C upon differentiation in defined medium without mitogens (Fig. 1B). Similar results were observed with c48 and pD (data not shown). In addition, both Nurr1 clones secreted significantly higher levels of TN-C protein compared with their respective control cell lines (data not shown). These results confirm that elevated Nurr1 levels in undifferentiated neural stem cells activate the expression of several genes (tubulin β III, neurofilament, and TN-C) that define a neuronal phenotype as identified by the microarray analysis. Next, we sought to determine whether the strong upregulation observed in Nurr1-expressing clones of TN-C was associated with Nurr1 expression. We addressed this by assessing TN-C transcript levels in ventral mesencephala isolated from E11 Nurr1-null embryos. Our quantitative PCR analysis indicates that ablation of Nurr1 expression resulted in diminished TN-C levels in vivo, confirming that TN-C is a downstream target of Nurr1 (Fig. 1C).

Nurr1 Overexpression Promotes Survival and Resistance to Oxidative Stress

The results of the GeneChip analysis revealed several trophic factors and survival signals upregulated by Nurr1, including transforming growth factor-β (TGF-β) and nerve growth factor (upregulated at least twofold in both clones). To assess whether

Table 1. Functional classification of genes upregulated in c17.2-Nurr1 stem cells

Protein	Function	Expression ratio		Accession no.
		c42/pB	c48/pD	
Extracellular matrix/cell structure				
Tenascin C	Differentiation	17.5	3.7	AV230686
H2A/H2B histones	Chromatin	8.2	2.5	X05862
β-Tubulin III	Cytoskeleton	4.0	3.4	AV350617
Neurofilament, medium polypeptide	Cytoskeleton	3.5	3.0	X05640
H1 histone	Chromatin	2.7	2.4	J03482
Transcription				
LRG-21/ATF3	Stress response	2.5	2.4	U19118
Engrailed-1	Homeodomain protein	2.4	2.4	L12703
Runx2	Differentiation	2.1	2.5	D14636
Slug	Differentiation	2.0	2.1	U79550
Peg1/MEST	Imprinting	1.6	23.6	AF017994
Secreted proteins				
Small inducible cytokine A7 (MCP-3)	Chemokine	20.7	1.5	X70058
Nerve growth factor β	Neurotrophin	5.4	2.5	M17298
Small inducible cytokine A2 (MCP-1)	Chemokine	4.3	1.4	M19681
IGFBP5 endopeptidase	Serine protease	3.3	2.4	AW125478
Stanniocalcin (Stc2)	Calcium homeostasis	2.6	2.3	AF031035
Wnt1-inducible secreted protein 1	Growth factor	2.1	2.7	AF100777
TGF-β	Growth factor	2.0	2.0	L19932
Other				
Interferon-inducible gene 202	Survival	5.6	1.6	M31418
ATP-binding cassette 1	Cholesterol efflux	3.2	2.6	AI845514
Unknown	Unknown	3.2	1.4	AW125508
Unknown	Unknown	2.1	2.7	AI844196

Genes commonly activated in two independent oligonucleotide chip comparisons between c17.2 Nurr1 neural stem cells (c42 and c48) and c17.2 control neural stem cells (pB and pD) were classified according to their known or putative function. Ratios represent the increase in gene expression.

Abbreviations: ATF, activating transcription factor; c, clone; IGFBP, insulin growth factor binding protein; MEST, mesoderm-specific transcript; pB, puroB; pD, puroD; TGF, transforming growth factor.

Table 2. Functional classification of genes downregulated in c17.2-Nurr1 stem cells

Protein	Function	Expression ratio		Accession no.
		c42/pB	c48/pD	
Extracellular matrix/cell structure				
Coagulation factor III	Coagulation	−4.7	−2.0	M26071
Integrin α4	Cell adhesion	−4.4	−2.6	X53176
Procollagen, type IV, α1	Cell adhesion	−3.6	−1.8	M15832
β-Filamin	Cytoskeleton/migration	−2.3	−2.0	AI838592
Myosin X	Cytoskeleton	−2.5	−2.4	AJ249706
Transcription/signaling				
ADP ribosyltransferase 3	Protein inactivation	−3.7	−1.7	Y08027
Prl3	Tyrosine phosphatase	−3.3	−1.7	AF035645
Brain fatty acid binding protein	Neural stem cell marker	−2.7	−6.4	U04827
Caspase-11	Apoptosis	−2.7	−2.2	Y13089
Ran GTPase activating protein-1	Cytoskeleton	−2.4	−2.2	U20857
Caspase-3	Apoptosis	−2.4	−1.8	U54803
ASM-like phosphodiesterase 3a	Ceramide release	−1.9	−4.4	Y08135
Eps8	Cytoskeleton	−1.8	−4.5	L21671
Myeloblastosis oncogene-like 1	Chromatin	−1.5	−3.5	L35261
Other				
Unknown	Unknown	−2.2	−2.3	AA797843
Zygin I	Membrane fusion	−1.6	−5.0	AI841076
Unknown	Unknown	−1.3	−4.1	AW121304

Genes commonly repressed in two independent oligonucleotide chip comparisons between c17.2 Nurr1 neural stem cells (c42 and c48) and c17.2 control neural stem cells (pB and pD) were classified according to their known or putative function. Ratios represent the decrease in gene expression.

Abbreviations: c, clone; pB, puroB; pD, puroD.

the trophic factors expressed by Nurr1-overexpressing cells were biologically active, conditioned medium from control and Nurr1-overexpressing cell lines was collected. Addition of conditioned medium from c42 or c48 cells to ventral mesencephalic E12.5 primary cultures increased the number of TH^+ dopaminergic neurons compared with the addition of conditioned medium from both control cell lines (Fig. 2A, 2B), suggesting that the trophic factors expressed by Nurr1 clones do indeed promote the survival and/or differentiation of DA neurons.

In addition to secreted factors, several survival, stress response/DNA repair, and antiapoptotic factors were also induced (e.g., LRG-21, gadd45β, and protein kinase C) in the Nurr1 clones. Notably, a number of proapoptotic genes were downregulated (e.g., ASM-like phosphodiesterase, Mekk1, caspase-3,

Table 3. Validation of microarray genes by quantitative PCR

	c42/pB		c48/pD	
	Affymetrix	RT-PCR	Affymetrix	RT-PCR
Secreted proteins				
WISP 1	2.1	2	2.7	3.7
IGFBP5 endopeptidase	3.3	9.1	2.4	5.4
Small inducible cytokine A2	4.3	3.1	1.4	1.9
Small inducible cytokine A7	20.7	4.6	1.5	2.2
Cell structure				
Neurofilament, medium peptide	3.5	1.2	3.0	5.5
H2A/H2B histones	8.2	−4	2.5	1.3
Signaling				
Caspase-11	−2.7	−1.5	−2.2	−1.7
Caspase-3	−2.4	−2.6	−1.8	−2.3
Transcription				
LRG-21/ATF3	2.5	9.1	2.4	2
Engrailed 1	2.4	4.5	2.4	1.0
Slug	2.0	3.2	2.1	2.5

Comparison of the expression ratio of selected genes, as calculated by Affymetrix GeneChip analysis and quantitative PCR. For quantitative PCR, specific primers were designed, and PCR values were normalized to the amplification value of the 18S housekeeping gene. Of 11 randomly selected genes, 10 were confirmed in independent cultures as Nurr1 NSCs.
Abbreviations: ATF, activating transcription factor; c, clone; IGFBP, insulin growth factor binding-protein; MEST, mesoderm-specific transcript; pB, puroB; pD, puroD; RT, reverse transcription; PCR, polymerase chain reaction.

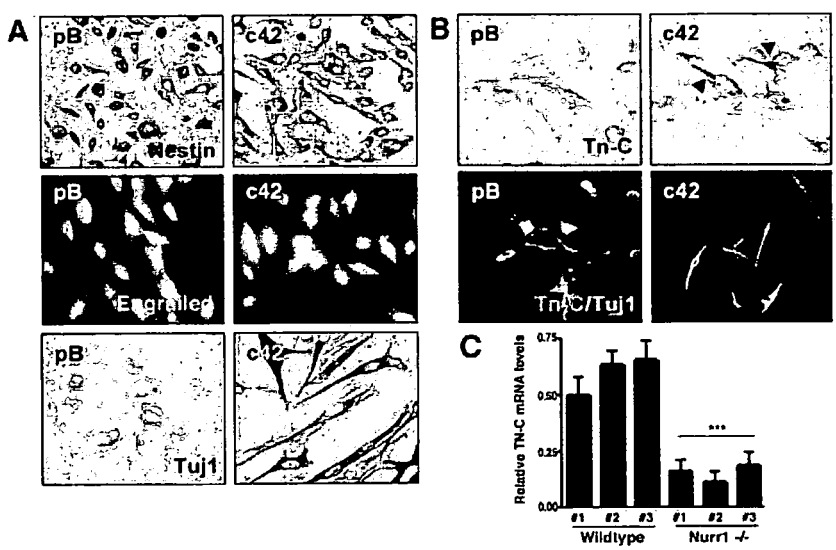

Figure 1. Nurr1 regulates the expression of stem/progenitor cell markers and promotes differentiation. (A, B): Immunocytochemical detection of Nestin, Engrailed-1, and Tuj1 (A) and tenascin-C (TN-C) (B) in both control (pB) and Nurr1 (c42) NSCs proliferating in the presence of serum. (B): Immunocytochemical detection of Tuj1 and TN-C in c42 differentiated for 3 days in the absence of serum. (C): TN-C transcripts levels were significantly reduced in the ventral mesencephala of Nurr1-null mice. For each experiment (n = 3), statistical analysis was performed using the paired t test (***, $p <$ .001). Abbreviations: c42, clone 42; pB, puroB; TN-C, tenascin-C; Tuj1, tubulin β III.

and caspase-11). An upregulation of several genes (e.g., oxidative stress-induced protein and cytochrome b5) involved in regulating the cellular response to oxidative stress was also observed (upregulated approximately 1.5-fold in both clones). Oxidative stress has been implicated in the pathophysiology of several neurodegenerative diseases, including PD [22–24]. We therefore examined whether Nurr1 expression protected cells from death induced by oxidative stress. Both sets of Nurr1-overexpressing neural stem cells and controls were treated with several concentrations of H_2O_2, and viable cells were counted after 6 hours. Peroxide treatments above 25 μM H_2O_2 were effective at inducing cell death in both sets of clones (data not shown). Cultures from both sets of control and Nurr1-overexpressing cells were treated with 25 μM peroxide and then stained with propidium iodide to identify dead cells. Significantly (40%) less cell death was observed in cells overexpressing Nurr1 compared with controls (Fig. 3A, 3B). To confirm the extent of apoptosis upon peroxide treatment, we assessed the presence of cleaved caspase-3 by immunocytochemistry. Fewer Nurr1-overexpressing cells were immunoreactive for cleaved caspase-3 compared with controls (Fig. 3C, 3D). Next, we examined whether Nurr1-overexpressing cells were resistant to peroxide-induced oxidative stress through secreted extrinsic factors or through cell-autonomous mechanisms. Control clones pB and pD were cultured with conditioned medium from Nurr1-expressing clones c42 and c48 and subjected to peroxide treatment. Conditioned medium from Nurr1 failed to rescue the peroxide-induced death associated with oxidative stress (data not shown). Together, these results demonstrate that Nurr1 promotes cell survival through secreted factors but helps confer resistance to oxidative stress through cell-intrinsic mechanisms by downregulating several proteins involved in the apoptotic response.

Premature Differentiation of DA Neurons in Tenascin-C-Null Mice

TN-C expression has been previously detected throughout the ventral mesencephalon from E9 to E13. However, the role of TN-C in the development of dopaminergic neurons remains largely unknown [25]. Our gene expression profiles suggested an important role for TN-C in developing DA neurons given its

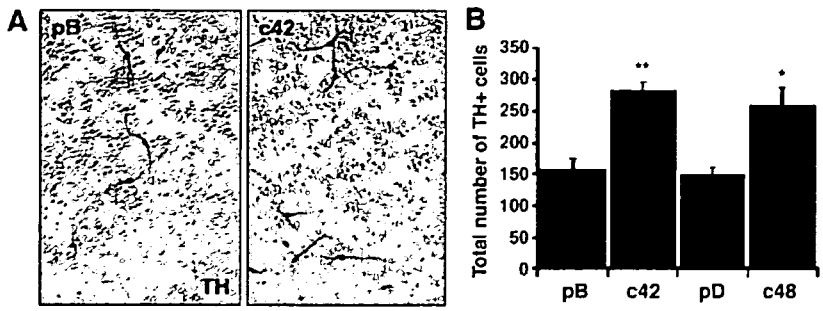

Figure 2. Nurr1 NSCs secrete trophic and survival signals that increase the number of dopaminergic neurons in mouse primary cultures. (A): Dissociated cells from embryonic day 12.5 (E12.5) mouse ventral mesencephala (VM) were treated with filtered N2 medium that had been conditioned by Nurr1 or control clones for 24h. Cells were fixed after 3 days in vitro and immunostained for TH. (B): Total numbers of TH^+ neurons in VM E12.5 primary cultures treated with conditioned medium. Values represent mean ± SEM of the total number of TH^+ cells per square centimeter of three independent experiments done in triplicate. Statistical analysis was performed by one-way analysis of variance with Fisher's post hoc test (*, $p < .05$; **, $p < .001$). Abbreviations: c42, clone 42; pB, puroB; pD, puroD; TH, tyrosine hydroxylase.

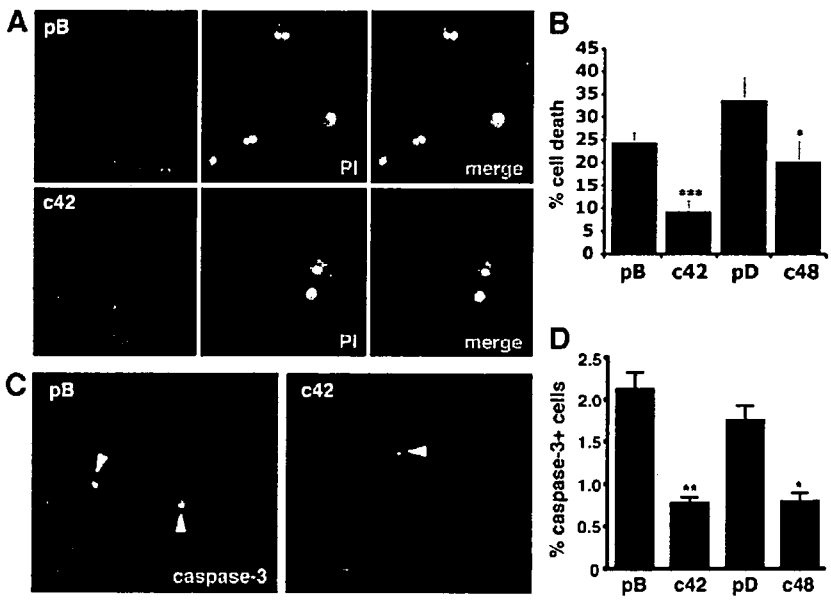

Figure 3. Nurr1 expression protects cells from oxidative stress-induced death. (A, B): Nurr1 clones were resistant to oxidative-stress induced death. Control and Nurr1 clones were treated with 25 μM H_2O_2 for 6 hours, stained with PI and Hoechst 33342, and counted ($n = 4$). Data represent the mean percent increase in cell death after 6 hours of peroxide treatment (Hoechst/PI). (C, D): Fewer Nurr1 NSCs were immunoreactive for cleaved caspase-3 following exposure to oxidative stress ($n = 4$). Statistical analysis was performed by one-way analysis of variance with Fisher's post hoc test (*, $p < .05$; **, $p < .001$; ***, $p < .0001$). Abbreviations: c42, clone 42; pB, puroB; pD, puroD; PI, propidium iodide.

upregulation in Nurr1 clones (Table 1). To investigate the role of TN-C in vivo, we analyzed tenascin-C knockout mice. At the onset of dopaminergic neurogenesis (E11), the number of tyrosine hydroxylase-immunoreactive cells was increased in TN-C-null mice (Fig. 4A, 4B). This increase was particularly confined to the more lateral dopaminergic neuron population. However, the excess of dopaminergic neurons was corrected for by E15 and postnatal day 1, a time period where neurogenesis has ended in vivo (Fig. 4B). We hypothesized that the early phenotype observed in TN-C knockouts could reflect an overproduction of proliferating DA progenitors or a change in the proliferative capacity of the ventral mesencephala. To assess this, we compared the numbers of proliferating cells between genotypes using BrdU, a marker that labels cells in the S phase of the cell cycle. BrdU analysis revealed no change in the number of proliferating cells in the ventral mesencephalon between the wild-type and TN-C-null mice at E11 (767.66 ± 59.88 and 708.00 ± 37.32, respectively; Fig. 4C) or E12.5 (data not shown). These results were further confirmed using an additional marker of proliferating cells, phosphorylated histone H3 (data not shown). Because the number of active caspase-3-immunoreactive cells did not differ between wild-type and TN-C-null mice (data not shown), these data suggest that deletion of TN-C does not increase the number of DA neurons by altering proliferation or cell survival. We next examined radial glia, cells that can act as stem cells and direct region-specific neural differentiation in the central nervous system [24, 26], including the developing midbrain (A.C. Hall et al., unpublished data). However, no change in RC2 or GLAST immunoreactivity was observed in TN-C-null mice at E11 (Fig. 4D; data not shown). In addition, TN-C knockout mice were analyzed for changes in $Nurr1^+$ DA precursors. At E11, no alterations in $Nurr1^+$ cells were observed between wild-type and TN-C knockout mice (Fig. 4D, 4E). These data indicate that TN-C normally acts to delay the acquisition of TH in $Nurr1^+$ precursors in vivo and that upon its deletion, the DA differentiation process is accelerated at E11, but the total number of TH^+ cells at the end of neurogenesis is not altered. Thus, our results suggest that $Nurr1^+$ cells, by regulating TN-C expression, delay their own differentiation into TH^+ neurons.

Discussion

To gain more insights into the molecular pathways regulated by Nurr1 during development, we performed an analysis of genes

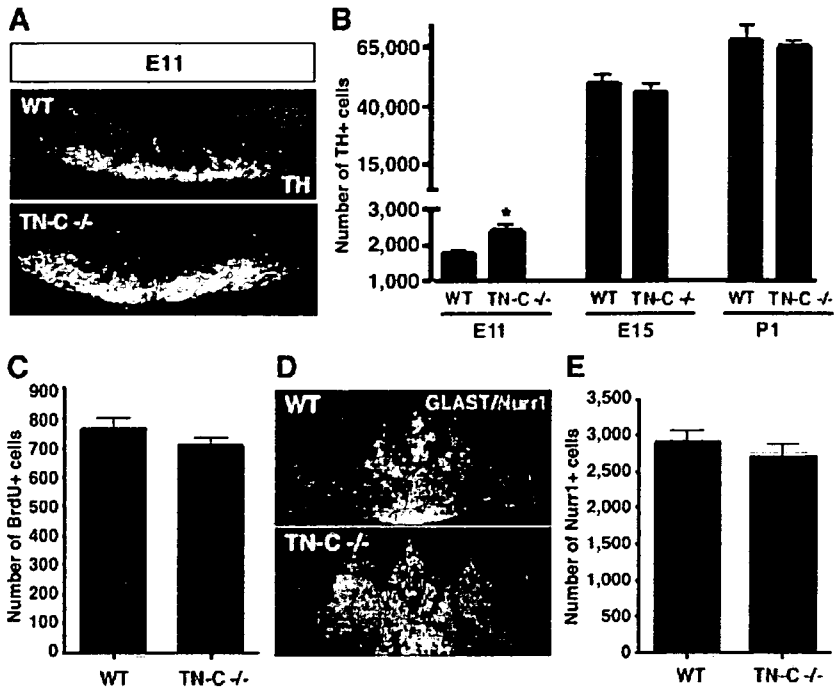

Figure 4. Tenascin-C-null mice display premature dopaminergic differentiation in vivo. **(A):** Coronal sections through embryonic day 11 (E11) ventral mesencephala (VM) revealed that the number of DA neurons (assessed by TH immunoreactivity) is increased in TN-C-null mice compared with controls. **(B):** Quantifications of TH^+ cells through serial coronal sections of E11, E15, and P1 control and TN-C-null mice. A correction in the number of TH^+ cells was observed by E15 and at P1 in TN-C-null mice. **(C):** Proliferating progenitors were identified by bromodeoxyuridine (BrdU) uptake in vivo at E11 in the VM. The proliferative capacity of E11 DA precursors was not affected in TN-C-null mice compared with control animals, as assessed by immunohistochemistry against BrdU. **(D, E):** The total numbers of $Nurr1^+$ cells and radial glia (GLAST) were not altered at E11 in TN-C-null mice compared with WT controls. For each experiment ($n = 5$), statistical analysis was performed using the paired t test (*, $p < .05$). Abbreviations: P1, postnatal day 1; TH, tyrosine hydroxylase; TN-C, tenascin-C; WT, wild-type.

regulated by Nurr1 in a proliferating neural stem cell line using Affymetrix microarrays. Of more than 12,000 genes queried, we identified approximately 400 genes that showed regulation by Nurr1. The findings we report here support a role for Nurr1 in reducing the potential of a neural stem/precursor cell by initiating its differentiation into a neuronal phenotype. Interestingly, this process was accompanied by an increase in the expression of genes that provide regional identity in the brain and confer cell survival and oxidative stress resistance. Thus, Nurr1 appears to coordinate the function of diverse genes during development.

The role of Nurr1 in promoting stem cell differentiation is supported by data from this microarray indicating that expression of neural stem cell markers, mitogens and their cognate receptors, and proteins that control cell cycle progression are downregulated (NCBI/GEO GSE3571). The downregulation of these genes could contribute to the coupling of cell cycle exit and differentiation programs in $Nurr1^+$ cells. Interestingly, Nurr1 induces cell cycle arrest and postmitotic maturation in cooperation with the cyclin dependent kinase inhibitor $p57^{kip2}$ in the dopamine-synthesizing neuronal cell line MN9D [27]. Accordingly, we have found several cell cycle genes downregulated in our study, in particular cyclin B2, D1, and p21 (all downregulated at least 1.5-fold in both comparisons and confirmed by quantitative PCR; data not shown).

Our results suggest that proliferating c17.2-Nurr1 cells represent a transition state from the multipotent neural stem cell to a precursor/immature neuron. Accordingly, the cytoskeletal protein encoding the neurofilament medium polypeptide was strongly induced in the Nurr1 clones. This result, together with the colocalization of tubulin β III (an early neuronal marker) and tenascin-C (involved in neurogenesis) in Nurr1 clones, suggests that proliferating c17.2-Nurr1 cells have initiated a precocious neuronal differentiation program. A strong repression of B-FABP expression was also detected: a fatty acid transporter that is highly expressed in neuroepithelial and radial glia cells in the developing brain and enriched in NSC cultures [28, 29]. Accordingly, the expression of several genes involved in non-neuronal development (such as that encoding the muscle cytoskeletal protein Myosin X, which is downregulated 2.5-fold in both clones) was repressed. Together, these results indicate that Nurr1 expression has positive effects on the development of a neuronal phenotype in NSCs.

Another important set of genes controlled by Nurr1 in a coordinated manner consists of those involved in promoting cell survival. Several studies have identified proteins critical for the induction and survival of mesencephalic dopaminergic neurons [30, 31]. Furthermore, retinoid X receptor (RXR) ligands that activate Nurr1-RXR heterodimers have been demonstrated to be critical for the survival of dopaminergic neurons [32]. Here, we observed an upregulation of several neurotrophic factors and downregulation of proapoptotic genes in Nurr1-overexpressing NSCs. Among the genes upregulated in Nurr1-overexpressing NSCs were two trophic signals required for the induction (TGF-β) and postnatal development (glial cell line-derived neurotrophic factor [GDNF]) of dopaminergic neurons [33, 34]. In fact, both TGF-β and GDNF have been shown to alleviate functional deficits in animal models of PD [35, 36]. Consistent with an upregulation of trophic factors was the observation that conditioned medium from c42 or c48 cells increased the number of TH^+ dopaminergic neurons in ventral mesencephalic E12.5 primary cultures compared with control conditioned medium. Our results suggest that Nurr1 overexpression induces the expression of several signals later required for the survival of dopaminergic neurons.

Moreover, both survival and stress response/DNA repair/antiapoptotic factors were induced (e.g., LRG-21 and gadd45β, upregulated 2.5- and 1.6-fold, respectively), whereas proapoptotic genes were downregulated (e.g., caspase-3, and caspase-11) in Nurr1 clones. Another gene regulated by Nurr1 in c17.2 cells was LRG-21, a member of the activating transcription factor/cAMP response element-binding protein family that is involved in the cellular stress response [37] and is regulated by seizures [38] and axotomy [39]. We also detected increased levels of gadd45β, an inducible factor that belongs to a protein family associated with cell-cycle control and DNA repair [40] and downregulates proapoptotic c-Jun N-terminal kinase signaling [41]. Thus, combined, our results indicate that one of the

main functions of Nurr1 is to promote survival by orchestrating the expression of stress response and antiapoptotic genes.

To further investigate the prosurvival effects of Nurr1, we examined whether Nurr1 expression protected cells from death induced by oxidative stress. The potential for oxidative damage is intrinsically associated with Nurr1$^+$/TH$^+$ dopaminergic neurons, since tyrosine hydroxylase activity forms oxygen radicals in a redox mechanism with its cofactor [42]. Cell survival upon oxidative treatments above 25 μM H_2O_2 was greater for Nurr1 clones compared with controls (Fig. 3A–3D). Microarray data indicating an upregulation in the expression of several oxidative-stress proteins important for maintaining free radical homeostasis in Nurr1-overexpressing cells (NCBI/GEO GSE3571) also supported these findings. Nurr1 NSCs also exhibited lower levels of cleaved caspase-3 protein after peroxide treatment compared with controls. This result is in agreement with previous findings showing that deletion of one Nurr1 allele decreases the survival of DA neurons in vitro [43] and that decreased Nurr1 expression increases the vulnerability of DA neurons to 1-methyl-4-phenyl-1,2,3,6-tetrahydropyridine (MPTP), a neurotoxin that induces oxidative stress and PD-like symptoms in rodents [14, 15, 24]. Nurr1 clones also expressed lower levels of caspase-11. Recent reports have indicated that caspase-11 knockout mice are more resistant to MPTP-mediated cell death than wild-type mice [44]. Moreover, the recent identification of Nurr1 mutations in PD patients [45] further suggests the intriguing possibility that the expression of survival and/or cell death genes regulated by Nurr1 could be altered in PD.

One of the highest induction rates in proliferating c17.2 Nurr1 NSCs corresponded to tenascin-C, an extracellular matrix glycoprotein. Tenascin-C is differentially expressed in specific patterns throughout nervous system, and although several genomic studies have previously implicated increased TN-C expression in maintaining the "stemness" of mouse neurospheres and rat neural progenitors, the precise role of TN-C remains unclear [46, 47]. Tenascin-C expression also correlates well with the migration, differentiation, and decreased proliferation of oligodendrocyte precursor cells, as well as axonal growth and guidance in neurons [48, 49]. Interestingly, analysis of TN-C levels in E11 Nurr1-null embryos revealed that TN-C is regulated by Nurr1 levels in vivo during dopaminergic neurogenesis (Fig. 1C). Moreover, adult mice lacking TN-C exhibit hyperlocomotive activities that have been attributed to altered levels of tyrosine hydroxylase and dopamine [17]. However, the observed increase in locomotor activity cannot be attributed to increased DA cell number since TN-C-null mice display higher numbers of DA neurons at the onset, but not at the end, of DA neurogenesis. Our results suggest the occurrence of a premature differentiation of Nurr1$^+$ precursors in TN-C-null mice at E11 that normalizes by E15. These data are in agreement with other findings showing normal phenotypes elsewhere later in development [49, 50]. Our data also indicate that at the onset of neurogenesis, TN-C does not regulate the size of the proliferative progenitor pool but instead contributes to preserving Nurr1$^+$ postmitotic precursors in a TH$^-$ state. Recent reports have described TN-C as a regulator of Wnt signaling [51]. Studies from our laboratory have also shown that Wnt signals and β-catenin overexpression regulate the maintenance and conversion of Nurr1$^+$ precursors into DA neurons [10, 52]. Thus, our results highlight a novel function for TN-C to maintain early Nurr1$^+$ postmitotic precursors in an undifferentiated state. These results further our understanding of how Nurr1 promotes neuronal differentiation.

ACKNOWLEDGMENTS

We thank Drs. Helder Andre, Clare Parish, Tibor Harkany, Carmen Salto, and Paola Sacchetti for critical reading and help with the manuscript. We also thank Jun Inoue for technical support, Dr. Dirk Koczan for help with the microarray data analysis, and Thomas Perlmann for providing Nurr1-null mice. Financial support was obtained from the Swedish Foundation for Strategic Research, Swedish Royal Academy of Sciences, Knut and Alice Wallenberg Foundation, Swedish Medical Research Council, Michael J. Fox Foundation, European Commission, Juvenile Diabetes Foundation, EuroStemCell, Karolinska Institute, and Petrus and Augusta Hedlunds Foundation. H.M. was supported by the Karolinska Institute. A.C.H. was supported by the Human Frontier of Science Program. K.M.S. and H.M. contributed equally to this work.

DISCLOSURES

E.A. owns stock in and has served as a scientific officer of and on the board of Neurotherapeutics AB within the last 2 years.

REFERENCES

1 Chung S, Sonntag KC, Andersson T et al. Genetic engineering of mouse embryonic stem cells by Nurr1 enhances differentiation and maturation into dopaminergic neurons. Eur J Neurosci 2002;16:1829–1838.
2 Kim JH, Auerbach JM, Rodriguez-Gomez JA et al. Dopamine neurons derived from embryonic stem cells function in an animal model of Parkinson's disease. Nature 2002;418:50–56.
3 Wagner J, Akerud P, Castro DS et al. Induction of a midbrain dopaminergic phenotype in Nurr1-overexpressing neural stem cells by type 1 astrocytes. Nat Biotechnol 1999;17:653–659.
4 Zetterstrom RH, Williams R, Perlmann T et al. Cellular expression of the immediate early transcription factors Nurr1 and NGFI-B suggests a gene regulatory role in several brain regions including the nigrostriatal dopamine system. Brain Res Mol Brain Res 1996;41:111–120.
5 Zetterstrom RH, Solomin L, Jansson L et al. Dopamine neuron agenesis in Nurr1-deficient mice. Science 1997;276:248–250.
6 Saucedo-Cardenas O, Quintana-Hau JD, Le WD et al. Nurr1 is essential for the induction of the dopaminergic phenotype and the survival of ventral mesencephalic late dopaminergic precursor neurons. Proc Natl Acad Sci U S A 1998;95:4013–4018.
7 Castillo SO, Baffi JS, Palkovits M et al. Dopamine biosynthesis is selectively abolished in substantia nigra/ventral tegmental area but not in hypothalamic neurons in mice with targeted disruption of the Nurr1 gene. Mol Cell Neurosci 1998;11:36–46.
8 Wallen A, Zetterstrom RH, Solomin L et al. Fate of mesencephalic AHD2-expressing dopamine progenitor cells in NURR1 mutant mice. Exp Cell Res 1999;253:737–746.
9 Hall AC, Mira H, Wagner J et al. Region-specific effects of glia on neuronal induction and differentiation with a focus on dopaminergic neurons. Glia 2003;43:47–51.
10 Castelo-Branco G, Wagner J, Rodriguez FJ et al. Differential regulation of midbrain dopaminergic neuron development by Wnt-1, Wnt-3a, and Wnt-5a. Proc Natl Acad Sci U S A 2003;100:12747–12752.
11 Snyder EY, Deitcher DL, Walsh C et al. Multipotent neural cell lines can engraft and participate in development of mouse cerebellum. Cell 1992;68:33–51.
12 Maruyama K, Tsukada T, Ohkura N et al. The NGFI-B subfamily of the nuclear receptor superfamily [Review]. Int J Oncol 1998;12:1237–1243.
13 Crispino M, Tocco G, Feldman JD et al. Nurr1 mRNA expression in neonatal and adult rat brain following kainic acid-induced seizure activity. Brain Res Mol Brain Res 1998;59:178–188.
14 Imam SZ, Jankovic J, Ali SF et al. Nitric oxide mediates increased susceptibility to dopaminergic damage in Nurr1 heterozygous mice. FASEB J 2005;19:1441–1450.

15 Le W, Conneely OM, He Y et al. Reduced Nurr1 expression increases the vulnerability of mesencephalic dopamine neurons to MPTP-induced injury. J Neurochem 1999;73:2218–2221.
16 Gritti A, Frolichsthal-Schoeller P, Galli R et al. Epidermal and fibroblast growth factors behave as mitogenic regulators for a single multipotent stem cell-like population from the subventricular region of the adult mouse forebrain. J Neurosci 1999;19:3287–3297.
17 Fukamauchi F, Mataga N, Wang YJ et al. Tyrosine hydroxylase activity and its mRNA level in dopaminergic neurons of tenascin gene knockout mouse. Biochem Biophys Res Commun 1997;231:356–359.
18 Fukamauchi F, Mataga N, Wang YJ et al. Abnormal behavior and neurotransmissions of tenascin gene knockout mouse. Biochem Biophys Res Commun 1996;221:151–156.
19 Joseph B, Wallen-Mackenzie A, Benoit G et al. p57(Kip2) cooperates with Nurr1 in developing dopamine cells. Proc Natl Acad Sci U S A 2003;100:15619–15624.
20 Arenas E. Stem cells in the treatment of Parkinson's disease. Brain Res Bull 2002;57:795–808.
21 Arenas E. Engineering a dopaminergic phenotype in stem/precursor cells: Role of Nurr1, glia-derived signals, and Wnts. Ann N Y Acad Sci 2005;1049:51–66.
22 Jenner P, Olanow CW. Oxidative stress and the pathogenesis of Parkinson's disease. Neurology 1996;47(suppl 3):161–170.
23 Klein JA, Ackerman SL. Oxidative stress, cell cycle, and neurodegeneration. J Clin Invest 2003;111:785–793.
24 Sherer TB, Greenamyre JT. Oxidative damage in Parkinson's disease. Antioxid Redox Signal 2005;7:627–629.
25 Kawano H, Ohyama K, Kawamura K et al. Migration of dopaminergic neurons in the embryonic mesencephalon of mice. Brain Res Dev Brain Res 1995;86:101–113.
26 Haubensak W, Attardo A, Denk W et al. Neurons arise in the basal neuroepithelium of the early mammalian telencephalon: A major site of neurogenesis. Proc Natl Acad Sci U S A 2004;101:3196–3201.
27 Castro DS, Hermanson E, Joseph B et al. Induction of cell cycle arrest and morphological differentiation by Nurr1 and retinoids in dopamine MN9D cells. J Biol Chem 2001;276:43277–43284.
28 Kurtz A, Zimmer A, Schnutgen F et al. The expression pattern of a novel gene encoding brain-fatty acid binding protein correlates with neuronal and glial cell development. Development 1994;120:2637–2649.
29 Conti L, Pollard SM, Gorba T et al. Niche-independent symmetrical self-renewal of a mammalian tissue stem cell. PLoS Biol 2005;3:e283.
30 Lin JC, Rosenthal A. Molecular mechanisms controlling the development of dopaminergic neurons. Semin Cell Dev Biol 2003;14:175–180.
31 Smidt MP, Smits SM, Burbach JP. Molecular mechanisms underlying midbrain dopamine neuron development and function. Eur J Pharmacol 2003;480:75–88.
32 Wallen-Mackenzie A, Mata de Urquiza A, Petersson S et al. Nurr1-RXR heterodimers mediate RXR ligand-induced signaling in neuronal cells. Genes Dev 2003;17:3036–3047.
33 Farkas LM, Dunker N, Roussa E et al. Transforming growth factor-beta(s) are essential for the development of midbrain dopaminergic neurons in vitro and in vivo. J Neurosci 2003;23:5178–5186.
34 Granholm AC, Reyland M, Albeck D et al. Glial cell line-derived neurotrophic factor is essential for postnatal survival of midbrain dopamine neurons. J Neurosci 2000;20:3182–3190.
35 Fernandez-Espejo E, El Banoua F, Caraballo I et al. Natural "dopaminotrophic" cell transplant: A new concept in antiparkinsonian therapy [in Spanish]. Rev Neurol 2003;36:540–544.
36 Gill SS, Patel NK, Hotton GR et al. Direct brain infusion of glial cell line-derived neurotrophic factor in Parkinson disease. Nat Med 2003;9:589–595.
37 Hai T, Hartman MG. The molecular biology and nomenclature of the activating transcription factor/cAMP responsive element binding family of transcription factors: Activating transcription factor proteins and homeostasis. Gene 2001;273:1–11.
38 Chen BP, Wolfgang CD, Hai T. Analysis of ATF3, a transcription factor induced by physiological stresses and modulated by gadd153/Chop10. Mol Cell Biol 1996;16:1157–1168.
39 Tsujino H, Kondo E, Fukuoka T et al. Activating transcription factor 3 (ATF3) induction by axotomy in sensory and motoneurons: A novel neuronal marker of nerve injury. Mol Cell Neurosci 2000;15:170–182.
40 Zhan Q, Antinore MJ, Wang XW et al. Association with Cdc2 and inhibition of Cdc2/Cyclin B1 kinase activity by the p53-regulated protein Gadd45. Oncogene 1999;18:2892–2900.
41 De Smaele E, Zazzeroni F, Papa S et al. Induction of gadd45beta by NF-kappaB downregulates pro-apoptotic JNK signalling. Nature 2001;414:308–313.
42 Adams JD Jr, Klaidman LK, Ribeiro P. Tyrosine hydroxylase: Mechanisms of oxygen radical formation. Redox Rep 1997;3:273–279.
43 Eells JB, Lipska BK, Yeung SK et al. Nurr1-null heterozygous mice have reduced mesolimbic and mesocortical dopamine levels and increased stress-induced locomotor activity. Behav Brain Res 2002;136:267–275.
44 Furuya T, Hayakawa H, Yamada M et al. Caspase-11 mediates inflammatory dopaminergic cell death in the 1-methyl-4-phenyl-1,2,3,6-tetrahydropyridine mouse model of Parkinson's disease. J Neurosci 2004;24:1865–1872.
45 Le WD, Xu P, Jankovic J et al. Mutations in NR4A2 associated with familial Parkinson disease. Nat Genet 2003;33:85–89.
46 Ramalho-Santos M, Yoon S, Matsuzaki Y et al. "Stemness": Transcriptional profiling of embryonic and adult stem cells. Science 2002;298:597–600.
47 Luo Y, Cai J, Liu Y et al. Microarray analysis of selected genes in neural stem and progenitor cells. J Neurochem 2002;83:1481–1497.
48 Joester A, Faissner A. The structure and function of tenascins in the nervous system. Matrix Biol 2001;20:13–22.
49 Garcion E, Faissner A, ffrench-Constant C. Knockout mice reveal a contribution of the extracellular matrix molecule tenascin-C to neural precursor proliferation and migration. Development 2001;128:2485–2496.
50 Garwood J, Garcion E, Dobbertin A et al. The extracellular matrix glycoprotein Tenascin-C is expressed by oligodendrocyte precursor cells and required for the regulation of maturation rate, survival and responsiveness to platelet-derived growth factor. Eur J Neurosci 2004;20:2524–2540.
51 Beiter K, Hiendlmeyer E, Brabletz T et al. beta-Catenin regulates the expression of tenascin-C in human colorectal tumors. Oncogene 2005;24:8200–8204.
52 Castelo-Branco G, Rawal N, Arenas E. GSK-3beta inhibition/beta-catenin stabilization in ventral midbrain precursors increases differentiation into dopamine neurons. J Cell Sci 2004;117:5731–5737.

See www.StemCells.com for supplemental material available online.

Microarray Analyses Support a Role for Nurr1 in Resistance to Oxidative Stress and Neuronal Differentiation in Neural Stem Cells

Kyle M. Sousa, Helena Mira, Anita C. Hall, Lottie Jansson-Sjöstrand, Moriaki Kusakabe and Ernest Arenas

Stem Cells 2007;25;511-519; originally published online Oct 12, 2006;
DOI: 10.1634/stemcells.2006-0238

The antiproliferative effects of agmatine correlate with the rate of cellular proliferation

Masato Isome, Mark J. Lortie, Yasuko Murakami, Eva Parisi, Senya Matsufuji and Joseph Satriano

Am J Physiol Cell Physiol 293:705-711, 2007. First published May 2, 2007;
doi:10.1152/ajpcell.00084.2007

Am J Physiol Cell Physiol 293: C705–C711, 2007.
First published May 2, 2007; doi:10.1152/ajpcell.00084.2007.

The antiproliferative effects of agmatine correlate with the rate of cellular proliferation

Masato Isome,[1] Mark J. Lortie,[1] Yasuko Murakami,[2] Eva Parisi,[1] Senya Matsufuji,[3] and Joseph Satriano[1,4]

[1]*Division of Nephrology-Hypertension and* [4]*The Stein Institute for Research on Aging, Department of Medicine, University of California San Diego and Veterans Affairs San Diego Healthcare System, La Jolla, California;* [2]*Department of Genetics and Molecular Biology, School of Pharmacy, Musashino University, Nishi-Tokyo, Japan; and* [3]*Department of Biochemistry II, The Jikei University School of Medicine, Tokyo, Japan*

Submitted 25 February 2007; accepted in final form 29 April 2007

Isome M, Lortie MJ, Murakami Y, Parisi E, Matsufuji S, Satriano J. The antiproliferative effects of agmatine correlate with the rate of cellular proliferation. *Am J Physiol Cell Physiol* 293: C705–C711, 2007. First published May 2, 2007; doi:10.1152/ajpcell.00084.2007.—Polyamines are small cationic molecules required for cellular proliferation. Agmatine is a biogenic amine unique in its capacity to arrest proliferation in cell lines by depleting intracellular polyamine levels. We previously demonstrated that agmatine enters mammalian cells via the polyamine transport system. As polyamine transport is positively correlated with the rate of cellular proliferation, the current study examines the antiproliferative effects of agmatine on cells with varying proliferative kinetics. Herein, we evaluate agmatine transport, intracellular accumulation, and its effects on antizyme expression and cellular proliferation in nontransformed cell lines and their transformed variants. H-ras- and Src-transformed murine NIH/3T3 cells (Ras/3T3 and Src/3T3, respectively) that were exposed to exogenous agmatine exhibit increased uptake and intracellular accumulation relative to the parental NIH/3T3 cell line. Similar increases were obtained for human primary foreskin fibroblasts relative to a human fibrosarcoma cell line, HT1080. Agmatine increases expression of antizyme, a protein that inhibits polyamine biosynthesis and transport. Ras/3T3 and Src/3T3 cells demonstrated augmented increases in antizyme protein expression relative to NIH/3T3 in response to agmatine. All transformed cell lines were significantly more sensitive to the antiproliferative effects of agmatine than nontransformed lines. These effects were attenuated in the presence of exogenous polyamines or inhibitors of polyamine transport. In conclusion, the antiproliferative effects of agmatine preferentially target transformed cell lines due to the increased agmatine uptake exhibited by cells with short cycling times.

polyamines; antizyme; ornithine decarboxylase; polyamine transport

POLYAMINES (PUTRESCINE, SPERMIDINE, AND SPERMINE) are required components for cellular proliferation (33, 52). Ornithine decarboxylase (ODC), one of the most highly regulated eukaryotic enzymes, is the first and rate-limiting enzyme of polyamine biosynthesis. It is a proto-oncogene that is significantly elevated in animal tumors (43, 44) and whose stepwise increase with the progression from normal colon mucosa to adenocarcinoma suggests a role in multistage carcinogenesis (21, 35, 37). Many of the same factors that induce ODC activity stimulate polyamine transport. As such, rapid polyamine uptake has been noted in many tumor cell lines compared with nontumorigenic cells of the same lineage (4, 15, 28, 31). In vivo,elevated plasma polyamine levels are associated with malignancy and tissue wasting, and tumor cells acquire polyamines released into the circulation (28). Selective inhibition of ODC with inhibitors such as 2-(difluoromethyl)-ornithine results in a compensatory increase in polyamine transport (4). Such upregulation of polyamine transport substitutes for de novo polyamine biosynthesis [for a review, see Ref. 50]. It is for these reasons that inhibition of ODC or the polyamine-converting enzymes alone have often complicated in vivo experimental interpretations as to the importance of polyamines and yielded less than anticipated results in clinical trials (17, 25, 28, 38, 45, 48). The importance of polyamine transport in addition to biosynthesis in affecting intracellular polyamine levels is now well established [for a review, see (49)]. Thus, beneficial intervention must be concerned with polyamine transport as well as biosynthesis when addressing intracellular polyamine availability for growth.

Intracellular polyamine levels are autoregulated via induction of the regulatory protein ODC antizyme (23). Induction of antizyme is via a programmed +1 ribosomal frameshift (23). This novel mechanism of translational induction affords rapid modulation in response to increased intracellular polyamine concentrations. As such, the cell is required to maintain constitutive levels of antizyme mRNA requisite for this response, which underscores the importance of this system in normal cell homeostasis. Four isoforms of antizyme have been described (22). Here, we refer to the most abundant, ubiquitous isoform, ODC antizyme-1. Antizyme binds to ODC, inhibits its activity and accelerates its degradation in a process catalyzed by the 26S proteasome (7, 13, 29). In addition to inhibiting polyamine biosynthesis, antizyme concurrently suppresses polyamine transporter activity (26, 51). This unique two-pronged negative feedback system is effective in limiting intracellular polyamine concentrations.

Arginine decarboxylase (ADC) converts arginine to agmatine. Intracellular concentrations of agmatine vary among organs, with high levels of synthesis and expression in kidney and liver (19, 20, 27). Agmatine inhibits proliferation by suppressing intracellular polyamine levels (1, 9, 42, 53). It induces antizyme expression via a programmed +1 ribosomal frameshift and is the only known endogenous molecule, other than the canonical polyamines, with this capacity (14, 42).

Address for reprint requests and other correspondence: J. Satriano, Univ. of California, San Diego, and Veterans Affairs San Diego Healthcare System, Div. of Nephrology-Hypertension, 3350 La Jolla Village Dr., San Diego, CA 92161 (e-mail: jsatriano@ucsd.edu).

The costs of publication of this article were defrayed in part by the payment of page charges. The article must therefore be hereby marked "*advertisement*" in accordance with 18 U.S.C. Section 1734 solely to indicate this fact.

Agmatine induces spermidine/spermine acetyltransferase in some cells types, which would promote the back-conversion of higher-order, more highly charged, to lower-order polyamines (53). It may also induce a yet unknown mechanism of suppressing ODC activity independent of antizyme (1). All of these mechanisms reduce intracellular polyamine pools and suppress growth.

We and others have shown that agmatine enters mammalian cells via the polyamine transporter (1, 3, 6, 40). As polyamine transport is positively correlated with proliferation rate, we examined whether agmatine preferentially targets rapidly proliferating, transformed cells (41). In this report, we investigate the effects of agmatine on primary, immortalized, transformed and tumorigenic cell lines and demonstrate that the antiproliferative effects correlate with the rate of proliferation in these cell lines.

MATERIALS AND METHODS

Materials. [^{3}H]Agmatine was purchased from American Radiolabeled Chemicals (St. Louis, MO). Polyamine transport inhibitors, MQT1202 (L-Lysine-Spermine) and MQT1483 [L-Lys(e-palmitoyl)-Spermine], were generous gifts from Drs. Reitha S. Weeks, Mark R. Burns, and MediQuest Therapeutics, (Seattle, WA) (5, 54). All other chemicals were purchased from Sigma (St. Louis, MO) unless otherwise noted.

Cells and cell culture. All cell lines were from American Type Culture Collection except Ha-ras (Ras/3T3)- and Src (Src/3T3)-transformed NIH/3T3 cells that were gifts from Dr. Mark Kamps (University of California, San Diego, San Diego, CA) (55), and the breast carcinoma cell lines N2O2 and PC7T were gifts from Dr. Daniel Gold of the Sidney Kimmel Cancer Center (San Diego, CA). Cell lines were maintained in Dulbecco's modified Eagle's medium (Cellgro, Herndon, VA) supplemented with 5% FBS (Atlanta Biologicals, Atlanta, GA), except primary fibroblast cells (CCD-1112Sk) that were maintained in Iscove's modified Eagle's media (Cellgro) supplemented with 5% FBS, unless otherwise noted.

Transport experiments. Monitoring intracellular transport was performed as previously described (39). Briefly, cells were grown in 6-well culture plates for 3 days until near confluence. Twenty-four hours before the uptake experiments, cells were placed in medium with limited (0.1%) FBS. Wells were washed with HEPES buffer (in mM): 25 Na^+-free HEPES, 5 KCl, 0.9 $CaCl_2$, 1 $MgSO_4$, 5.6 D-glucose, 137 NaCl. The addition of HEPES buffer containing 10 μM [^{3}H]agmatine at ~200,000 cpm/well started the 30-min uptake period. Three rapid washes with ice-cold PBS and lysis in 3N NaOH terminated the reactions. Bio-Rad Protein Assay (Bio-Rad, Hercules, CA) used a small aliquot of each lysate for protein determination; the remainder of the sample was counted in a β-scintillation counter to evaluate uptake. Uptake at 4°C, representing nonspecific binding and diffusional transport, was subtracted from the above determinations.

Intracellular agmatine determination. Cells were plated on 10-cm culture dishes. Twenty-four hours before extraction, the cells were placed in serum-free medium, except the primary fibroblast cell line, which required 0.1% FBS. Eight hours after medium change, 100 μM agmatine was added to the experimental samples for a 16-h uptake period at 37°C. Cells were then washed with ice-cold PBS and lysed in 10% TCA in 10 mM HCl. The sample supernatants were transferred to a 10,000 molecular weight spin filter (Millipore) for further purification, and then they were extracted three times with hydrated ethyl ether to remove traces of TCA and lipids. Cell extracts and standards were derivatized for fluorescence detection of primary and secondary amine groups with *N*-hydroxysuccinimidyl-6-aminoquinoyl carbamate as per kit instructions (AccQ tag; Waters, Franklin, MA). Elution was performed using a Hewlett-Packard 1100 series binary HPLC pump system with a 250-mm 3-μm ODS Hypersil C18 RP column (Hewlett-Packard) maintained at 45°C. Fluorescence was detected in line using a Waters 470 detector linked to the data acquisition system. Elution gradients were based on the AccQ tag kit instructions.

Cell counting. Cells were plated for the days indicated in 10-cm culture dishes or 6-well plates, washed with PBS, and harvested in trypsin/EDTA for quantification in a Coulter Counter (model ZM). In experiments in which cells were preloaded with putrescine, 250 μM putrescine was added to the cells 3 h before the addition of agmatine. Polyamine transport inhibitors MQT1202 (1 μM) and MQT1483 (1 μM) were also added 3 h before agmatine administration.

Western blot analysis. For Western blot analysis, Ras/3T3 cells were collected and lysed [lysis buffer: 1% triton-X 100, 0.5% deoxycholic acid, 1 mM EDTA, 0.1% SDS, 4 mM NaF, Complete protease cocktail (Roche Molecular Biochemicals, Mannheim, Germany), 0.7 μg/ml pepstatin and 1 mM $NaVO_4$ in PBS]. Lysates were resolved on 12% NuPAGE gels in MOPS buffer (Invitrogen, Carlsbad, CA). Gel proteins were transferred to nitrocellulose membranes and immunoblotted with antizyme-1 antibody (24). This antibody cross-reacts weakly with mouse antizyme-2 (data not shown). The secondary antibody was horseradish peroxidase-conjugated (Santa Cruz Biotechnology, Santa Cruz, CA) for autoradiographic detection by ECL Plus (Amersham Pharmacia, Piscataway, NJ), with densitometric analysis by ImageJ Software (National Institutes of Health, Bethesda, MD).

Determination of antizyme activity. The cells were washed with ice-cold PBS and disrupted by three freeze-thaw cycles. Then, 0.5 ml of extract buffer (25 mM Tris·HCl, pH 7.4, 1 mM DTT, and 0.01% Tween 80) was added, and the cell suspension was centrifuged at 18,000 *g* for 20 min at 4°C. The supernatant contained both active free ODC and inactive ODC bound to antizyme (ODC-antizyme complex). Free ODC activity was assayed by measuring the release of $^{14}CO_2$ from L-[1-^{14}C] ornithine. The basal reaction mixture contained 0.0625 mCi of L-[1-^{14}C]ornithine, 0.4 mM L-ornithine, 40 mM pyridoxal phosphate, 5 mM DTT, 40 mM Tris·HCl buffer, pH 7.4, 0.01% Tween 80 and enzyme solution in a final volume of 125 ml. Inactive ODC (ODC-antizyme complex) was determined as the increase in ODC activity caused by the addition of an excess amount of recombinant GST fusion antizyme inhibitor (0.1 mg) to the basal reaction mixture described above. Antizyme activity was equated to the amount of ODC-antizyme complex.

Statistical evaluations. Variations between samples within groups were analyzed by ANOVA, with significance determined by Fisher's protected least significant differences post hoc test. StatView software (ver. 4.5; Abacus Concepts, Berkeley, CA) was used for these analyses. All data are means (SD) and represent at least three separate determinations.

RESULTS

Transport and accumulation of agmatine in cell lines. An increased rate of cellular proliferation is associated with increased polyamine uptake. We and others have shown that agmatine import into mammalian cells uses the polyamine transport system (1, 6, 40, 41). Although epithelial cells are primarily chosen for proliferation studies because of their prevalence in cancer, plasticity in epithelial tumor cells toward a fibroblastoid phenotype in progression toward metastasis, that is, an epithelial-mesenchymal transition, is now well established (12). Furthermore, polyamine transport is well characterized in fibroblast cell lines and display a single polyamine transporter in both murine and human (49, 50). Cell lines include the murine fibroblast NIH/3T3 line, NIH/3T3 cells transformed by stable transfection of either H-ras or Src, in Ras/3T3 or Src/3T3 cells, respectively (55), a primary human foreskin fibroblast line (cell designation CCD 1112Sk,

from the American Type Culture Collection, Manassas, VA) and the human fibrosarcoma cell line HT1080.

Growth curves of the cell lines over a 4-day period are shown in Fig. 1. After replating, the cells have a lag phase before assuming log phase growth from *day 3*. The largest differences were observed at *day 4*. The transformed Ras/3T3, Src/3T3, and HT1080, cell lines grew more rapidly than their nontransformed or primary culture counterparts.

Transport of agmatine significantly increases in transformed Ras/3T3 and Src/3T3 cells relative to the parental murine NIH/3T3 cell line (Fig. 2*A*). Cellular uptake of agmatine also appreciably increases in human fibrosarcoma cells, HT1080, relative to the primary fibroblast cell line. We observe a significant increase in agmatine import from nontransformed to transformed variants of mammalian cell lines, regardless of whether the cells are of murine or human origin.

HPLC analysis shows an accumulation of intracellular agmatine levels that increase after incubation with 100 μM agmatine for 16 h in transformed cell lines relative to the primary and immortalized lines in a pattern similar to that of agmatine transport (Fig. 2*B*). The potential of agmatine within the cell depends not only on import, but also on export and metabolism. The equilibrium of these components is represented by the intracellular accumulation of agmatine. Baseline levels of agmatine in cells in culture are very low to undetectable, so we assume the effects observed are due to addition of exogenous agmatine.

Preferential suppression of growth by agmatine in transformed cells. Preferential uptake and accumulation of agmatine into transformed cell lines suggest that these cell lines would be more responsive to the antiproliferative effects of agmatine. We evaluated cell growth, as a function of accrued cell number after 4 days in the presence of agmatine relative to untreated control cells, the latter being set to 100% (Fig. 3). All transformed cell lines demonstrated a significant decrease in cell number relative to their untreated controls by 50 μM agmatine, immortalized NIH/3T3 cells by 250 μM agmatine, and primary fibroblasts were not significantly affected by agmatine within this concentration range. The SV40 transformed the renal proximal tubule cell line, and MCT, displayed a similar sensitivity to agmatine as exhibited here by the transformed variants (42).

Polyamine supplementation or inhibition of polyamine transport suppresses the effects of agmatine. We preloaded Ras/3T3 cells with the polyamine putrescine and evaluated the effects of agmatine on cell growth, as per Fig. 3. Addition of putrescine to Ras/3T3 cells attenuated the antiproliferative effects of agmatine (Fig. 4*A*). Competitive inhibition of agmatine uptake by putrescine would also contribute to this effect. Uptake rates of agmatine and putrescine are quite similar in these cells (40). At equimolar concentrations of agmatine and putrescine, that is, at 250 μM, would yield a 50% inhibition of agmatine uptake. The effects of putrescine administration are far greater than can be accounted for by competitive inhibition alone. These data support earlier work that the antiproliferative effects observed with agmatine are due in large part to polyamine depletion (42).

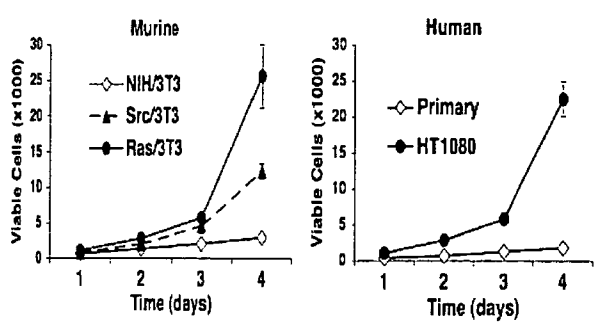

Fig. 1. Cell line growth profiles. Proliferative kinetics of cell lines plated at equal densities over 4 days. Primary, primary foreskin fibroblast cell line.

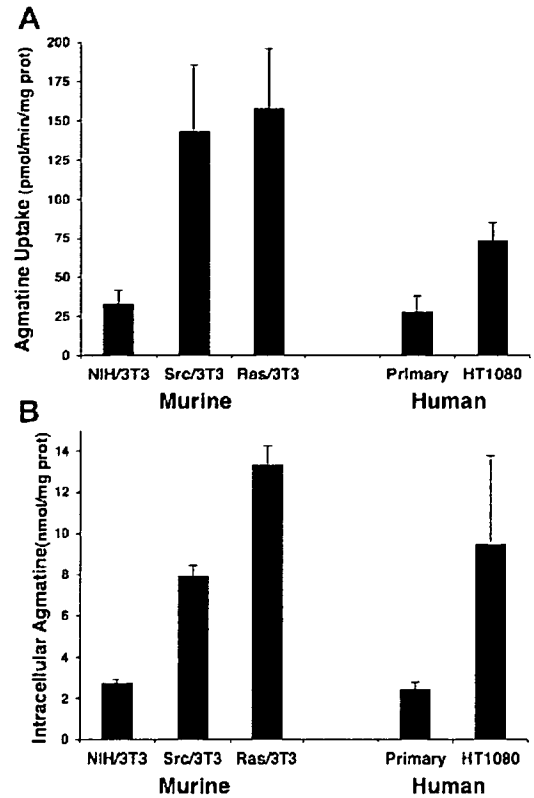

Fig. 2. Changes in agmatine uptake rate and accumulation in cell lines. *A*: uptake of 10 μM [^{3}H]agmatine into the cell lines. *B*: HPLC determination of intracellular agmatine concentrations in the presence of 100 μM agmatine. There were significant and parallel differences between parental NIH/3T3 cell lines vs. Ras/3T3 and Src/3T3 transformed varients, as with primary fibroblast cells vs. HT1080 fibrosarcoma cells ($P < 0.05$).

We next evaluated the significance of the polyamine transport system on the antiproliferative effects of agmatine. Administration of the polyamine transport inhibitors MQT1202 and MQT1483 prevented the inhibitory effects of agmatine on Ras/3T3 cells (Fig. 4*B*). Thus, polyamine transporters are required for significant import of agmatine into these cells to produce antiproliferative effects.

Effects of agmatine on induction of antizyme. Induction of antizyme occurs in many cell types in response to agmatine administration. Increased uptake of agmatine into the more rapidly proliferating transformed cells should affect antizyme induction, assuming that antizyme function and/or induction is not desensitized by transformation. NIH/3T3, Ras/3T3, and Src/3T3 cells were grown for 4 days in the absence or presence of agmatine (250 μM and 500 μM) and antizyme expression

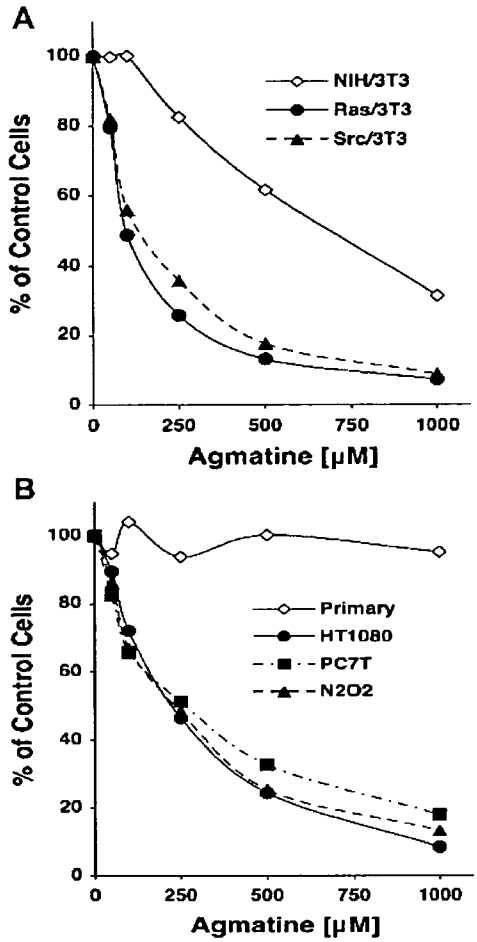

Fig. 3. Selective antiproliferative effects of agmatine on cell lines of murine (*A*), or human origin (*B*). Cells were plated and allowed to grow for 4 days in the concentrations of agmatine indicated. Cell number was evaluated in a Coulter Counter. Untreated, control cells of all cell lines were placed at 100%. N_2O_2 and PC7T beast carcinoma cell lines were added to this study to broaden the scope of responses to agmatine.

evaluated by Western blot analysis (Fig. 5*A*). Antizyme expression consistently increased to a greater degree in the transformed cell lines in response to agmatine administration than the parental NIH/3T3 cell line. Putrescine (250 μM), agmatine (1 mM), or a combination of the two-increased antizyme protein expression in Ras/3T3 cells (Fig. 5*B*). Increases in antizyme in response to agmatine administration were confirmed in antizyme activity assays (not shown).

DISCUSSION

The differential uptake and accumulation of agmatine in transformed relative to nontransformed cell lines correlate with the antiproliferative effects of agmatine. Oncogene transformed murine cells, Ras/3T3 and Src/3T3, and human fibrosarcoma, HT1080, exhibit accelerated growth rates, higher agmatine uptake, and intracellular agmatine concentrations, and they are more sensitive to the antiproliferative effects of agmatine than are their respective immortalized, NIH/3T3, or primary fibroblast counterparts. Two breast carcinoma cell lines, N2O2 and PC7T, also displayed a high sensitivity to agmatine, similar to the fibrosarcoma cell line, HT1080. Akin to the canonical polyamines, agmatine is a cationic molecule with amine groups that are subject to acetylation. This process neutralizes the charge of the molecules and facilitates their cellular export. Unlike the simple amines of polyamines, the guanidino group of agmatine may allow for a different intracellular localization (2) and make it less prone to cellular export.

The kidney, liver, brain, and adrenals maintain high constitutive levels of ADC activity (20, 27). Although ADC was localized to the mitochondrial membrane, agmatine generation was not observed in mitochondrial extracts (8). This is contrary to findings in whole organ preparations (20) and requires further examination. Whether sourced from the gut flora or biosynthesis within organs, agmatine is widely distributed within the plasma (2.8 μM; see Ref. 19) and extracellular fluid and can be selectively concentrated in several organs (19, 36).

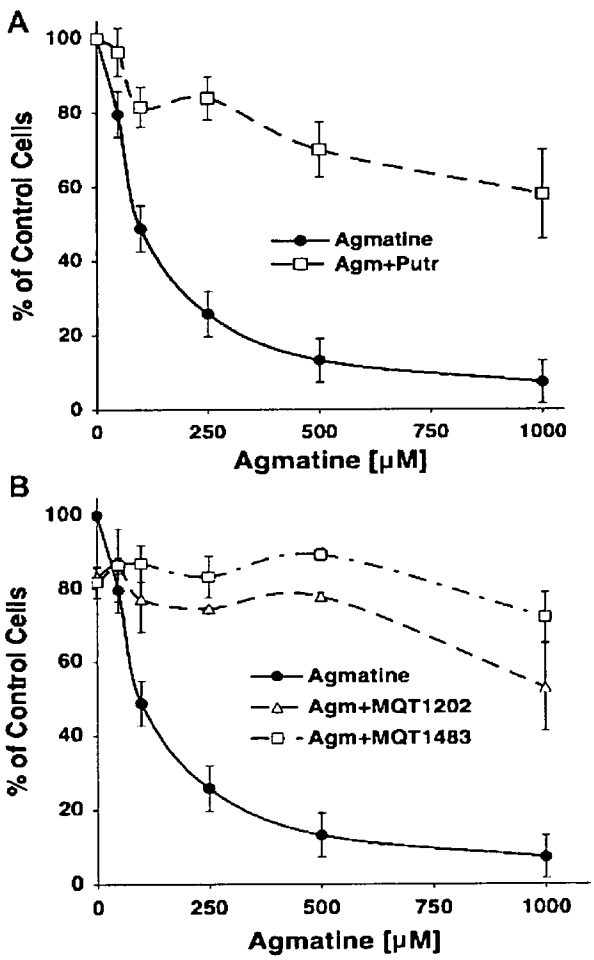

Fig. 4. The effects of agmatine are suppressed by polyamine supplementation or inhibition of polyamine transport. *A*: Ras/3T3 cells were preincubated with putrescine (Putr; 250 μM) for 3 h before the administration of agmatine. The cells were incubated in the absence or presence of putrescine and/or agmatine, and cell number per well was determined as per Fig. 2*B*. *B*: Ras/3T3 cells were incubated with the polyamine transport inhibitor MQT1202 or MQT1483 at a concentration of 1 μM for 3 h before the administration of agmatine and throughout the remainder of the experiment. The cell number per well was determined as above.

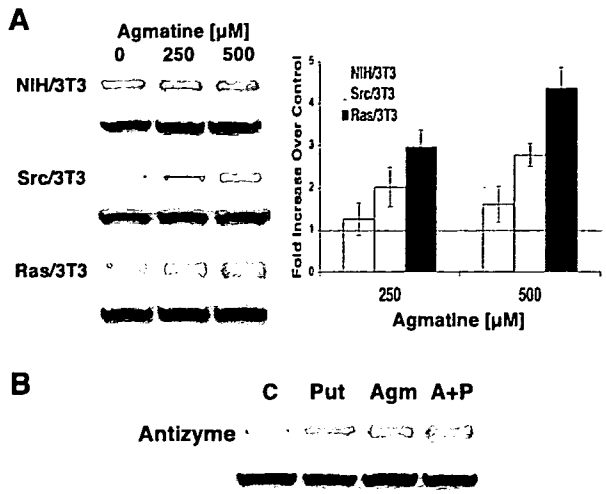

Fig. 5. Variations in antizyme expression in the presence of agmatine. *A*: Antizyme protein evaluation by Western blot analysis of NIH/3T3, Src/3T3, and Ras/3T3 cells treated with agmatine for 4 days at the concentrations indicated. The graph represents antizyme protein expressed as a fold increase observed with agmatine over untreated control values (straight line). Ras/3T3 and Src/3T3 cell lines were significantly different from their respective controls, and NIH/3T3 cells at 250 μM and 500 μM agmatine concentrations ($P < 0.05$). NIH/3T3 cells were different from its untreated controls at 500 μM agmatine ($P < 0.05$). *B*: Western blot analysis for antizyme protein expression in Ras/3T3 cells cultured in the absence, control (C), or presence of 250 μM putrescine (Put), 1 mM agmatine (Agm), or a combination of agmatine and putrescine (A+P), for 4 days. Evaluation of β-actin expression to demonstrate protein loading is shown below the appropriate antizyme bands in both *A* and *B* of this figure.

Concentrations of agmatine in early reports were underestimated due to the lability of the molecule in the derivatization process, a problem that has not been entirely eradicated. More recently, the tissue level of agmatine in the rat kidney was reported to approximate over 400 μM (19). In all of the cell lines evaluated in this report, the growth rates of transformed cells treated with 50 μM agmatine were significantly different from their untreated controls, with a maximal effect at ~500 μM. Rat hepatoma cells, HTC, exhibit a similar profile in response to agmatine with a significance at 50 μM and maximal effects at 500 μM (personal communication, Sebastiano Colombatto, University of Torino, Italy).

Expression of antizyme is primarily controlled at the translational level through ribosomal frameshifting, although there is also a transcriptional mechanism when polyamines are depleted (30). However, there has been no evidence that the polyamine dose response/frameshift kinetics are altered by malignant transformation. The polyamine concentrations required for maximal frameshift efficiency, and the degree of frameshift efficiency was the same in transformed MCT cells as reported for normal rat liver (23, 42). Immunoprecipitation of antizyme from agmatine-treated MCT cell preparations prevented the inhibitory effects on ODC activity (42). We show that agmatine significantly increases antizyme protein levels in two transformed cell lines and also that loading cells with putrescine reduces the effects of agmatine on proliferation. The antiproliferative effects of agmatine thus appear due to polyamine depletion and not due to agmatine functionally replacing or displacing the canonical polyamines (42). Agmatine appears to require cellular import for its antiproliferative effects. It is a multifunctional molecule with both receptor-dependent and -independent functions. As import is required (Fig. 4*B*), the antiproliferative effects evaluated in this study appear receptor independent. Furthermore, exogenously administered putrescine or agmatine imported into the cytosol induces antizyme expression (Fig. 5*B*). These studies are in accord with studies demonstrating temporal translocation and compartmentalization of ODC and antizyme (11, 34, 47). Taken together, these data would suggest a mechanism whereby the rapid conversion and utilization of polyamines may result in lower unbound or "free" cytosolic polyamine levels that are insufficient to induce antizyme expression, and/or how the inhibitor may be unable to reach the enzyme, depending upon the physiological status of the cell. However, this hypothesis cannot be directly substantiated by current techniques. We do show that exogenously administered putrescine or agmatine, which imports into the cytosol, is capable of inducing antizyme expression.

Agmatine would be complementary, that is, additive, to the endogenous polyamine pool and thereby effectively lower the threshold levels of polyamines required to bring about the translational induction of antizyme. In addition, induction of antizyme by agmatine could constitute a self-limiting feedback mechanism by inhibiting both polyamine and agmatine uptake (Fig. 6). Taken together, these observations suggest that the polyamine feedback system in these transformed cells is functional, but it may be evaded in proliferating cells. This is not to say that regulation of antizyme expression is not altered in some neoplasms (18, 46) but suggests that such alteration is not as universal in neoplasia as is increased ODC activity. Several studies support the view that induction of antizyme may prove to be a viable method of attenuating neoplastic growth (10, 16, 18, 32).

In summary, the preferential antiproliferative effects of agmatine on several transformed mammalian cell lines occurs from enhanced cellular uptake by polyamine transporters, and subsequent suppression of proliferation. This process exploits the upregulation of polyamine transporters in rapidly cycling cells and may be a useful template for drug development.

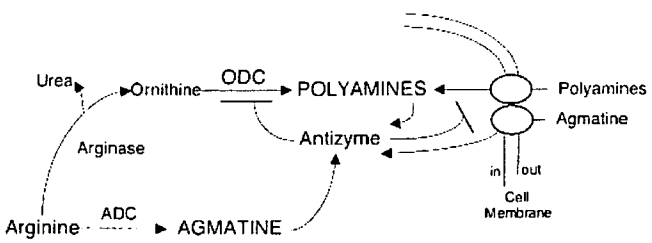

Fig. 6. Proposed mechanism. Rapidly dividing cells upregulate polyamine transport. Intracellular agmatine accumulation by synthesis and/or transport mediates antizyme induction. Antizyme suppresses intracellular polyamine levels by inhibiting polyamine synthesis and transport and limits further agmatine uptake through the polyamine transporter. Agmatine may also induce spermidine/spermine acetyltransferase activity and reduce ornithine decarboxylase (ODC) activity independent of antizyme (not illustrated). These mechanisms would also reduce intracellular polyamine content. Bars represent negative regulation; ovals in cell membrane symbolize polyamine transporters. ADC, arginine decarboxylase.

ACKNOWLEDGMENTS

Eva Parisi is a visiting scholar from the Nephrology Research Laboratory IRBLLEIDA, Hospital Universitari Arnau de Vilanova, Rovira Roure 80. 1ª Planta, 25198, Lleida, Spain.

Present address of Dr. M. Isome: Department of Pediatrics, Fukushima Medical University, School of Medicine1, Hikarigaoka Fukushima-City, Fukushima 960-1295, Japan.

GRANTS

This work was supported by National Institutes of Health Grants DK-070123, DK-070667, DK-02920, DK-56248, DK-28602, the American Cancer Society, University of California, San Diego, Cancer Center Grant, the Stein Institute for Research on Aging, Center Grant, and funds supplied by the Research Service of the Department of Veterans Affairs.

REFERENCES

1. **Babal P, Ruchko M, Campbell CC, Gilmour SP, Mitchell JL, Olson JW, Gillespie MN.** Regulation of ornithine decarboxylase activity and polyamine transport by agmatine in rat pulmonary artery endothelial cells. *J Pharmacol Exp Ther* 296: 372–377, 2001.
2. **Babal P, Ruchko M, Olson JW, Gillespie MN.** Interactions between agmatine and polyamine uptake pathways in rat pulmonary artery endothelial cells. *Gen Pharmacol* 34: 255–261, 2000.
3. **Blantz RC, Satriano J, Gabbai F, Kelly C.** Biological effects of arginine metabolites. *Acta Physiol Scand* 168: 21–25, 2000.
4. **Bogle RG, Mann GE, Pearson JD, Morgan DM.** Endothelial polyamine uptake: selective stimulation by L-arginine deprivation or polyamine depletion. *Am J Physiol Cell Physiol* 266: C776–C783, 1994.
5. **Burns MR, Carlson CL, Vanderwerf SM, Ziemer JR, Weeks RS, Cai F, Webb HK, Graminski GF.** Amino acid/spermine conjugates: polyamine amides as potent spermidine uptake inhibitors. *J Med Chem* 44: 3632–3644, 2001.
6. **Cabella C, Gardini G, Corpillo D, Testore G, Bedino S, Solinas SP, Cravanzola C, Vargiu C, Grillo MA, Colombatto S.** Transport and metabolism of agmatine in rat hepatocyte cultures. *Eur J Biochem* 268: 940–947, 2001.
7. **Coffino P.** Polyamines in spermiogenesis: not now, darling [comment]. *Proc Natl Acad Sci USA* 97: 4421–4423, 2000.
8. **Coleman CS, Hu G, Pegg AE.** Putrescine biosynthesis in mammalian tissues. *Biochem J* 379: 849–855, 2004.
9. **Dudkowska M, Lai J, Gardini G, Stachurska A, Grzelakowska-Sztabert B, Colombatto S, Manteuffel-Cymborowska M.** Agmatine modulates the in vivo biosynthesis and interconversion of polyamines and cell proliferation. *Biochim Biophys Acta* 1619: 159–166, 2003.
10. **Feith DJ, Shantz LM, Pegg AE.** Targeted antizyme expression in the skin of transgenic mice reduces tumor promoter induction of ornithine decarboxylase and decreases sensitivity to chemical carcinogenesis. *Cancer Res* 61: 6073–6081, 2001.
11. **Gritli-Linde A, Nilsson J, Bohlooly YM, Heby O, Linde A.** Nuclear translocation of antizyme and expression of ornithine decarboxylase and antizyme are developmentally regulated. *Dev Dyn* 220: 259–275, 2001.
12. **Grunert S, Jechlinger M, Beug H.** Diverse cellular and molecular mechanisms contribute to epithelial plasticity and metastasis. *Nat Rev Mol Cell Biol* 4: 657–665, 2003.
13. **Hayashi S, Murakami Y, Matsufuji S.** Ornithine decarboxylase antizyme: a novel type of regulatory protein. *Trends Biochem Sci* 21: 27–30, 1996.
14. **Higashi K, Yoshida K, Nishimura K, Momiyama E, Kashiwagi K, Matsufuji S, Shirahata A, Igarashi K.** Structural and functional relationship among diamines in terms of inhibition of cell growth. *J Biochem (Tokyo)* 136: 533–539, 2004.
15. **Holley JL, Mather A, Wheelhouse RT, Cullis PM, Hartley JA, Bingham JP, Cohen GM.** Targeting of tumor cells and DNA by a chlorambucil-spermidine conjugate. *Cancer Res* 52: 4190–4195, 1992.
16. **Iwata S, Sato Y, Asada M, Takagi M, Tsujimoto A, Inaba T, Yamada T, Sakamoto S, Yata J, Shimogori T, Igarashi K, Mizutani S.** Antitumor activity of antizyme which targets the ornithine decarboxylase (ODC) required for cell growth and transformation. *Oncogene* 18: 165–172, 1999.
17. **Janne J, Alhonen L, Leinonen P.** Polyamines: from molecular biology to clinical applications. *Ann Med* 23: 241–259, 1991.
18. **Koike C, Chao DT, Zetter BR.** Sensitivity to polyamine-induced growth arrest correlates with antizyme induction in prostate carcinoma cells. *Cancer Res* 59: 6109–6112, 1999.
19. **Lortie MJ, Ishizuka S, Schwartz D, Blantz RC.** Bioactive products of arginine in sepsis: tissue and plasma composition after LPS and iNOS blockade. *Am J Physiol Cell Physiol* 278: C1191–C1199, 2000.
20. **Lortie MJ, Novotny WF, Peterson OW, Vallon V, Malvey K, Mendonca M, Satriano J, Insel P, Thomson SC, Blantz RC.** Agmatine, a bioactive metabolite of arginine. Production, degradation, and functional effects in the kidney of the rat. *J Clin Invest* 97: 413–420, 1996.
21. **Luk GD, Baylin SB.** Ornithine decarboxylase as a biologic marker in familial colonic polyposis. *N Engl J Med* 311: 80–83, 1984.
22. **Mangold U.** The antizyme family: polyamines and beyond. *IUBMB Life* 57: 671–676, 2005.
23. **Matsufuji S, Matsufuji T, Miyazaki Y, Murakami Y, Atkins JF, Gesteland RF, Hayashi S.** Autoregulatory frameshifting in decoding mammalian ornithine decarboxylase antizyme. *Cell* 80: 51–60, 1995.
24. **Matsufuji S, Miyazaki Y, Kanamoto R, Kameji T, Murakami Y, Baby TG, Fujita K, Ohno T, Hayashi S.** Analyses of ornithine decarboxylase antizyme mRNA with a cDNA cloned from rat liver. *J Biochem (Tokyo)* 108: 365–371, 1990.
25. **McCann PP, Pegg AE.** Ornithine decarboxylase as an enzyme target for therapy. *Pharmacol Ther* 54: 195–215, 1992.
26. **Mitchell JL, Judd GG, Bareyal-Leyser A, Ling SY.** Feedback repression of polyamine transport is mediated by antizyme in mammalian tissue-culture cells. *Biochem J* 299: 19–22, 1994.
27. **Morrissey J, McCracken R, Ishidoya S, Klahr S.** Partial cloning and characterization of an arginine decarboxylase in the kidney. *Kidney Int* 47: 1458–1461, 1995.
28. **Moulinoux JP, Quemener V, Khan NA.** Biological significance of circulating polyamines in oncology. *Cell Mol Biol* 37: 773–783, 1991.
29. **Murakami Y, Matsufuji S, Hayashi S, Tanahashi N, Tanaka K.** Degradation of ornithine decarboxylase by the 26S proteasome. *Biochem Biophys Res Commun* 267: 1–6, 2000.
30. **Nilsson J, Koskinieni S, Persson K, Grahn B, Holm I.** Polyamines regulate both transcription and translation of the gene encoding ornithine decarboxylase antizyme in mouse. *Eur J Biochem* 250: 223–231, 1997.
31. **Pegg AE.** Polyamine metabolism and its importance in neoplastic growth and a target for chemotherapy. *Cancer Res* 48: 759–774, 1988.
32. **Pegg AE, Feith DJ, Fong LY, Coleman CS, O'Brien TG, Shantz LM.** Transgenic mouse models for studies of the role of polyamines in normal, hypertrophic and neoplastic growth. *Biochem Soc Trans* 31: 356–360, 2003.
33. **Pegg AE, McCann PP.** Polyamine metabolism and function. *Am J Physiol Cell Physiol* 243: C212–C221, 1982.
34. **Pomidor MM, Ruhl KK, Zheng P, Song Y, Janne OA, Tuan RS, Hickok NJ.** Relationship between ornithine decarboxylase and cytoskeletal organization in cultured human keratinocytes: cellular responses to phorbol esters, cytochalasins, and alpha-difluoromethylornithine. *Exp Cell Res* 221: 426–437, 1995.
35. **Porter CW, Herrera-Ornelas L, Pera P, Petrelli NF, Mittelman A.** Polyamine biosynthetic activity in normal and neoplastic human colorectal tissues. *Cancer* 60: 1275–1281, 1987.
36. **Raasch W, Regunathan S, Li G, Reis DJ.** Agmatine, the bacterial amine, is widely distributed in mammalian tissues. *Life Sci* 56: 2319–2330, 1995.
37. **Radford DM, Nakai H, Eddy RL, Haley LL, Byers MG, Henry WM, Lawrence DD, Porter CW, Shows TB.** Two chromosomal locations for human ornithine decarboxylase gene sequences and elevated expression in colorectal neoplasia. *Cancer Res* 50: 6146–6153, 1990.
38. **Redgate ES, Boggs S, Grudziak A, Deutsch M.** Polyamines in brain tumor therapy. *J Neurooncol* 25: 167–179, 1995.
39. **Satriano J, Ishizuka S, Archer DC, Blantz RC, Kelly CJ.** Regulation of intracellular polyamine biosynthesis and transport by NO and cytokines TNF-alpha and IFN-gamma. *Am J Physiol Cell Physiol* 276: C892–C899, 1999.
40. **Satriano J, Isome M, Casero RA Jr, Thomson SC, Blantz RC.** Polyamine transport system mediates agmatine transport in mammalian cells. *Am J Physiol Cell Physiol* 281: C329–C334, 2001.
41. **Satriano J, Kelly CJ, Blantz RC.** An emerging role for agmatine. *Kidney Int* 56: 1252–1253, 1999.
42. **Satriano J, Matsufuji S, Murakami Y, Lortie MJ, Schwartz D, Kelly CJ, Hayashi S, Blantz RC.** Agmatine suppresses proliferation by frameshift induction of antizyme and attenuation of cellular polyamine levels. *J Biol Chem* 273: 15313–15316, 1998.

43. **Scalabrino G, Ferioli ME.** Polyamines in mammalian tumors. Part I. *Adv Cancer Res* 35: 151–268, 1981.
44. **Scalabrino G, Ferioli ME.** Polyamines in mammalian tumors. Part II. *Adv Cancer Res* 36: 1–102, 1982.
45. **Schechter PJ, Barlow JLR, Sjoerdsma A.** Clinical aspects of inhibition of ornithine decarboxylase with emphasis on therapeutic trials of eflornithine (DFMO) in cancer and protozoan diseases. In: *Inhibition of Polyamine Metabolism*, edited by McCann PP, Pegg AE, and Sjoerdsma A. Orlando, FL: Academic, 1987, p. 345–367.
46. **Schipper RG, Romijn JC, Cuijpers VM, Verhofstad AA.** Polyamines and prostatic cancer. *Biochem Soc Trans* 31: 375–380, 2003.
47. **Schipper RG, Verhofstad AA.** Distribution patterns of ornithine decarboxylase in cells and tissues. Facts, problems, and postulates. *J Histochem Cytochem* 50: 1143–1160, 2002.
48. **Seiler N.** Pharmacological properties of the natural polyamines and their depletion by biosynthesis inhibitors as a therapeutic approach. *Prog Drug Res* 37: 107–159, 1991.
49. **Seiler N, Delcros JG, Moulinoux JP.** Polyamine transport in mammalian cells. An update. *Int J Biochem Cell Biol* 28: 843–861, 1996.
50. **Seiler N, Dezeure F.** Polyamine transport in mammalian cells. *Int J Biochem* 22: 211–218, 1990.
51. **Suzuki T, He Y, Kashiwagi K, Murakami Y, Hayashi S, Igarashi K.** Antizyme protects against abnormal accumulation and toxicity of polyamines in ornithine decarboxylase-overproducing cells. *Proc Natl Acad Sci USA* 91: 8930–8934, 1994.
52. **Tabor CW, Tabor H.** Polyamines. *Annu Rev Biochem* 53: 749–790, 1984.
53. **Vargiu C, Cabella C, Belliardo S, Cravanzola C, Grillo MA, Colombatto S.** Agmatine modulates polyamine content in hepatocytes by inducing spermidine/spermine acetyltransferase. *Eur J Biochem* 259: 933–938, 1999.
54. **Weeks RS, Vanderwerf SM, Carlson CL, Burns MR, O'Day CL, Cai F, Devens BH, Webb HK.** Novel lysine-spermine conjugate inhibits polyamine transport and inhibits cell growth when given with DFMO. *Exp Cell Res* 261: 293–302, 2000.
55. **White FC, Benehacene A, Scheele JS, Kamps M.** VEGF mRNA is stabilized by ras and tyrosine kinase oncogenes, as well as by UV radiation—evidence for divergent stabilization pathways. *Growth Factors* 14: 199–212, 1997.

Available online at www.sciencedirect.com
ScienceDirect
Journal of Colloid and Interface Science 318 (2008) 440–448
JOURNAL OF Colloid and Interface Science
www.elsevier.com/locate/jcis

Adsorption and micellization behavior of novel gluconamide-type gemini surfactants

Kenichi Sakai [a,*], Shin Umezawa [b], Mamoru Tamura [b], Yuichiro Takamatsu [c], Koji Tsuchiya [a], Kanjiro Torigoe [a], Takahiro Ohkubo [d,1], Tomokazu Yoshimura [e], Kunio Esumi [b,d], Hideki Sakai [a,d], Masahiko Abe [a,d]

[a] *Department of Pure and Applied Chemistry, Faculty of Science and Technology, Tokyo University of Science, 2641 Yamazaki, Noda, Chiba 278-8510, Japan*
[b] *Department of Applied Chemistry, Faculty of Science, Tokyo University of Science, 1-3 Kagurazaka, Shinjuku, Tokyo 162-8601, Japan*
[c] *Miyoshi Oil & Fat Co., Ltd., 4-66-1 Horikiri, Katsushika, Tokyo 124-8510, Japan*
[d] *Institute of Colloid and Interface Science, Tokyo University of Science, 1-3 Kagurazaka, Shinjuku, Tokyo 162-8601, Japan*
[e] *Graduate School of Humanities and Sciences, Nara Women's University, Kitauoyanishi-machi, Nara 630-8506, Japan*

Received 4 September 2007; accepted 25 October 2007

Available online 6 November 2007

Abstract

The adsorption and micellization behavior of novel sugar-based gemini surfactants (N,N'-dialkyl-N,N'-digluconamide ethylenediamine, Glu(n)-2-Glu(n), where n is the hydrocarbon chain length of 8, 10 and 12) has been studied on the basis of static/dynamic surface tension, fluorescence, dynamic light scattering (DLS) and cryogenic transmission electron microscope (cryo-TEM) data. The static surface tension of the aqueous Glu(n)-2-Glu(n) solutions measured at the critical micelle concentration (cmc) is observed to be significantly lower than that of the corresponding monomeric surfactants. This suggests that the gemini surfactants, newly synthesized in the current study, are able to form a closely packed monolayer film at the air/aqueous solution interface. The greater ability in the molecular association is supported by the remarkably (approximately 100–200 times) lower cmc of the gemini surfactants compared with the corresponding monomeric ones. With a combination of the fluorescence and DLS data, a structural transformation of the Glu(n)-2-Glu(n) micelles is suggested to occur with an increase in the concentration. The cryo-TEM measurements clearly confirm the formation of worm-like micelles of Glu(12)-2-Glu(12) at the concentration well above the cmc.

Keywords: Sugar-based gemini surfactants; Adsorption; Worm-like micelles; Surface tension

1. Introduction

Gemini surfactants, consisting of two monomeric surfactants linked with a spacer, have been synthesized with a view to developing 'next-generation' high-quality surfactants. When compared with a conventional monomeric surfactant, the corresponding gemini surfactants generally present, e.g., (i) a significantly lower critical micelle concentration (cmc), (ii) a lower surface tension recorded at the cmc and (iii) a greater ability in increasing viscosity of the diluted aqueous solution [1–3]. Indeed, a structural transformation from spherical micelles to vesicles is observed even in a diluted aqueous solution of gemini surfactants, being reflective of their larger packing parameter [4] than that of the corresponding monomeric surfactants. Although the synthetic process of gemini surfactants is generally more complicated than that of monomeric ones (and thereby, the synthetic costs are still problematic), these physicochemical properties of gemini surfactants may reduce the total consumption of substances in chemical products. Therefore, gemini surfactants themselves are deemed to be an environment-friendly material.

From the standpoint of human health and ecology, sugar-based nonionic surfactants are also an important and possible

* Corresponding author.
E-mail address: k-sakai@rs.noda.tus.ac.jp (K. Sakai).
[1] Current address: Division of Chemistry and Biochemistry, Graduate School of Natural Science and Technology, Okayama University, 3-1-1 Tsushimanaka, Okayama 700-8530, Japan.

0021-9797/$ – see front matter
doi:10.1016/j.jcis.2007.10.039

alternative over conventional surfactants [5,6]. It is generally accepted that there is a cloud point in an aqueous solution of polyoxyethylene alkyl ether surfactants, however, no precipitation or phase separation is seen once the sugar-based surfactants are molecularly dissolved in water [7,8]. With the expectation for the biodegradability, non-toxicity and biocompatibility, the absence of the cloud point enables us to use the sugar-based surfactants in a wide variety of applications such as detergents, dish-washing agents and personal care products [9,10]. During the last decade gemini surfactants containing sugar moieties in their headgroups have been synthesized and the aqueous solution properties have been studied: one typical series of this type of gemini surfactants is made from monosaccharides (or their derivatives) [11–20] and the other is made from disaccharides (or their derivatives) [13,14,21]. In addition, sugar-based gemini surfactants with a disaccharide spacer have been synthesized by Menger and Mbadugha [22].

Recently we also synthesized two types of sugar-based gemini surfactants: one is a series of the cationic-nonionic hetero-gemini surfactants with a glucono-lactone (monosaccharide) derived headgroup [23] and the other is a series of the non-ionic disaccharide-based surfactants synthesized from lactobionic acid [24]. The latter surfactants enabled us to report that the cmc value becomes remarkably lower (approximately 1/10–1/200) than that of the corresponding monomeric surfactants, as expected. When compared at a given hydrocarbon chain length, however, the surface tension measured above the cmc was found to be much greater for the gemini surfactants than for the monomeric ones. Indeed, the occupied area per hydrocarbon chain adsorbed at the air/aqueous solution interface was estimated to be significantly larger for the gemini surfactants than for the corresponding monomeric ones. The lower surface activity of the disaccharide-based gemini surfactants used in our previous study may arise from the bulky structure: the spacer of the surfactants was hexanediamide and the sugar-based headgroups were connected with the tertiary amine group via an ethylene-peptide unit ($-CH_2CH_2-NHCO-$). We believe, therefore, that sugar-based gemini surfactants having a less bulky structure are desirable for an excellent surface activity (as well as the biodegradability and so on).

Herein we focus on the adsorption/micellization behavior of novel sugar-based gemini surfactants synthesized from glucono-lactone (monosaccharide), Glu(n)-2-Glu(n) (N,N'-dialkyl-N,N'-digluconamide ethylenediamine, where n is the hydrocarbon chain length of 8, 10 and 12). The chemical structure of Glu(n)-2-Glu(n) is given in Fig. 1. Note that the monosaccharide moieties are directly bound to the tertiary amine group at the level of the ethylene spacer. As far as we are aware, this particular structure is new and thereby the physicochemical properties observed at the air/aqueous solution interface and/or in aqueous solution are worth reporting. The adsorption properties at the air/aqueous solution interface has been assessed with static/dynamic surface tensiometry, whereas the micellization behavior has been monitored with fluorescence, dynamic light scattering (DLS) and cryogenic transmission electron microscope (cryo-TEM) measurements.

2. Experimental

2.1. Materials

For the synthesis of Glu(n)-2-Glu(n) we used ethylenediamine (Kanto Chemical Co., Inc.), 1-bromooctane, 1-bromodecane, 1-bromododecane, D-(+)-glucono-1,5-lactone (Tokyo Chemical Industry Co., Ltd.), methanol, ethanol, 1-propanol, acetone, hexane, diethylether and acetonitrile (Wako Pure Chemical Industries Ltd.). Note that the chemicals listed above were of analytical grade and used without further purification.

The corresponding monomeric surfactants, N-alkyl-N-methylgluconamide (Glu(n): $n = 10$ and 12), were synthesized in accordance with the procedure reported previously [6]. These monomeric surfactants were used for dynamic surface tension, fluorescence and DLS measurements. The water used in the current study was of Millipore Milli-Q grade.

2.2. Synthesis

The final products, Glu(n)-2-Glu(n) ($n = 8$, 10 and 12), were synthesized via the following 2 steps (see also Fig. 1). The products obtained at each step were characterized with ^{1}H NMR

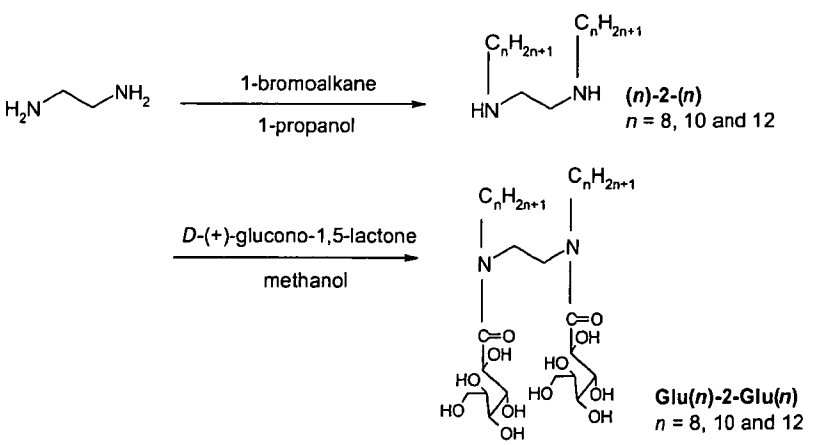

Fig. 1. Synthetic route of Glu(n)-2-Glu(n) ($n = 8$, 10 and 12).